Metal Ion-Induced Self-Assembly of Functionalized 2,6-Oligopyridines. 2. Copper-Containing Double-Stranded Helicates Derived from Functionalized Quaterpyridine and Quinquepyridine: Redox State-Induced Transformations and Electron Communication in Mixed-Valence Systems[1a]

Kevin T. Potts,*,† Majid Keshavarz-K,† Fook S. Tham,† Héctor D. Abruña,*,‡ and Claudia R. Arana‡

Departments of Chemistry, Rensselaer Polytechnic Institute, Troy, New York 12181, and Cornell University, Ithaca, New York 14853

Received March 9, 1993

Spontaneous self-assembly of functionalized quaterpyridines and quinquepyridines at ambient temperature in the presence of an appropriate copper ion resulted in a versatile group of multimetallic, double-stranded helical complexes. Methylthio-substituted quaterpyridine and copper ion gave a bimetallic complex with Cu(I) and a monometallic complex with Cu(II). Redox state-induced transformations between these complexes were demonstrated chemically and verified spectroelectrochemically. The $[LCu^{I}]_2[PF_6]_2$ complex crystallized in the monoclinic space group $I2/a$ (No. 15) with unit cell dimensions $a = 17.021(4)$ Å, $b = 16.212(4)$ Å, $c = 20.303(4)$ Å, $\beta = 103.09(2)°$, $V = 5457(2)$ Å^3, and $Z = 2$. The X-ray data showed that the two ligand strands intertwined about each other and around the two distorted tetrahedral metal ions in a double-helical fashion, with the Cu–Cu distance being 3.32 Å. Alkylthio-substituted quinquepyridines formed homo- and mixed-valence, bimetallic and also trimetallic helical complexes in quantitative yield at ambient temperature, depending on the nature of the metal ion and that of a supplementary ligand and the reaction conditions. Redox state-induced transformations between these complexes were also demonstrated chemically and verified spectroelectrochemically. The trimetallic complex in acetonitrile showed three reversible, one-electron oxidations at +1.03(70), +0.50(50), and –0.04(60) V attributed to three Cu(I)/Cu(II) couples. The significant difference in oxidation potentials ($\Delta E°' = 530$ and 540 mV) is indicative of metal–metal interactions in this homometallic complex, and ^{1}H NMR studies established its high symmetry and chiral nature. The homovalence $[L_2Cu^{II}_2OAc][PF_6]_3$ complex crystallized in the orthorhombic space group *Pbnn* (No. 52) with unit cell dimensions $a = 16.558(3)$ Å, $b = 16.684(3)$ Å, $c = 25.577(4)$ Å, $\alpha = \beta = \gamma = 90°$, $V = 7066(2)$ Å^3, and $Z = 4$, and the X-ray data showed its double-stranded helical nature, the metal ions having distorted octahedral geometry and different chemical environments (N_6 and N_4O_2) with a supplementary bidentate acetate ligand completing the coordination sphere of one of the Cu(II) ions. The Cu–Cu distance was 4.44 Å. The $[L_2Cu^{II}/Cu^{I}][PF_6]_3$ mixed-valence complex crystallized in the monoclinic space group $I2/a$ (No. 15) with unit cell dimensions $a = 25.002(6)$ Å, $b = 15.501(4)$ Å, $c = 33.560(6)$ Å, $\beta = 91.09(2)°$, $V = 13004(4)$ Å^3, and $Z = 8$, and the X-ray data showed a similar helical arrangement of the ligand about the two copper ions, which had distorted octahedral and distorted tetrahedral geometry, respectively, with a Cu–Cu distance being 4.25 Å. An intervalence electron-transfer (IT) transition between the mixed-valence copper centers showed broad absorption centered at 1414 nm [$\epsilon = 70$ (cm M)$^{-1}$] is clear evidence for electron delocalization and metal–metal coupling between the two copper centers in this complex.

Introduction

A previous paper[1b] in this series described synthetic sequences leading to a variety of substituted bipyridines through decipyridines designed to include peripheral substituents chosen to enhance ligand solubility, to allow for new functional group introduction, and to be amenable to NMR study. In this article we describe procedures for effecting the high-yield Cu(I) and Cu(II) ion-induced self-assembly of a new, functionalized quaterpyridine **1b** (mt-qtpy; mt = methylthio) and quinquepyridine **4a** (mt-qnpy) and **4b** (pt-qnpy; pt = *n*-propylthio) to form several multimetallic, double stranded-helical complexes (helicates).[2] A detailed analysis of their complex redox properties shows that significant metal–metal interaction occurs in several of these helicates. Subsequent publications will describe additional coordination and electrochemistry of these ligands and similarly substituted sexipyridines with other transition metals and extend our study to septipyridine and octipyridine.

Oligopyridines joined through their 2,6-positions have the ability to accommodate different coordination numbers preferred by a particular metal ion and are thus excellent precursors to multimetallic complexes with different coordination geometries. Electronic communication between redox active sites in these multimetallic complexes is of considerable interest, and their potential application in the assembly of molecular wires and other electroactive or electronic devices appears promising.[3]

Multidentate ligands that lack preorganization may bind to a metal center in a variety of ways. Quaterpyridine, a tetradentate ligand that assumes a transoid conformation in both the solid state and in solution,[1b,6a] is capable of acting as a planar tetradentate ligand to coordinate to a single metal cation and a

† Rensselaer Polytechnic Institute.
‡ Cornell University.

(1) (a) Abstracted in part from the Ph.D. dissertations of M.K. (RPI), 1993, and C.A. (Cornell), 1992. (b) For part 1 of this series see: Potts, K. T.; Gheysen Raiford, K. A.; Keshavarz-K, M. *J. Am. Chem. Soc.* **1993**, *115*, 2793. (c) Presented in part at the European Colloquium on Heterocyclic Chemistry, Toledo, Spain, 1990 (Potts, K. T. *Bull. Soc. Chem. Belg.* **1990**, *99*, 741).

(2) For recent references to this topic that refer to earlier literature see: (a) Pfeil, A.; Lehn, J.-M. *J. Chem. Soc., Chem. Commun.* **1992**, 838. Lehn, J.-M. *Angew. Chem., Int. Ed. Engl.* **1990**, *29*, 1304. (b) Ruthmann, S.; Pigriet, C.; Bernardinelli, G.; Bocquet, B.; Williams, A. F. *J. Am. Chem. Soc.* **1992**, *114*, 4230.

(3) For a recent discussions see: (a) Whitesides, G. M.; Mathias, J. P.; Seto, C. T. *Science* **1991**, *254*, 1312. (b) *Frontiers in Supramolecular Organic Chemistry and Photochemistry*; Schneider, J.; Dürr, H., Eds.; VCH: Weinheim, Germany, 1991. (c) *Molecular Electronic Devices*; Carter, F. L., Ed.; Marcel Dekker: New York, 1982; Part II, 1987.

(4) Maslin, E. N.; Raston, C. L.; White, A. H. *J. Chem. Soc., Dalton Trans.* **1975**, 323.

(5) Henke, W.; Kremer, S.; Reinen, D. *Z. Anorg. Allg. Chem.* **1982**, *491*, 124.

0020-1669/93/1332-4422$04.00/0

bis(bidentate) ligand to coordinate to two metal cations, as well as a terdentate and monodentate ligand to coordinate one or two metal cations. Although significant strain energy, clearly evident from molecular models (CPK), is associated with a planar tetradentate coordination of quaterpyridine (**1c**) to a single first-row metal cation, a number of such complexes have been isolated and studied. The structural analysis of $[Co(qtpy)(H_2O)(SO_3)][NO_3]\cdot H_2O$ showed[4] that the qtpy ligand was behaving as a planar tetradentate although the complex is asymmetric, with the inner nitrogen–cobalt bonds being shorter than the outer ones by some 0.12 Å. Crystal structure analyses of $[Co(qtpy)(H_2O)(NO_3)][NO_3]\cdot H_2O$, $[Co(qtpy)(H_2O)_2][NO_3]_2$, $[Ni(qtpy)(CH_3CN)_2][PF_6]_2$, and $[Pd(qtpy)][PF_6]_2$ have also been described[5,6] with the ligand acting in planar tetradentate fashion in all cases.

It has also been shown[7] that the partially preorganized 3,5′,3″,5‴-tetramethyl-2,2′:6′,2″:6″,2‴-quaterpyridine (**1a**), designed to act as a bis(bidentate) ligand due to the steric hindrance of the methyl groups at the 5′- and 3″-positions, underwent ready reaction with Cu(I) perchlorate to yield a double-stranded helicate **2a**. X-ray data established that the two Cu(I) cations bound by the two ligand strands had a distorted tetrahedral coordination geometry. However the same ligand formed a square pyramidal complex **3a** with Cu(II), also established[7] by X-ray data. A very recent report described[8] the formation of related double-stranded helicates from both Cu(I) and Ag(I) and quaterpyridine itself.

Addition of an extra ligating center to **1**, resulting in the quinquepyridines, increases the number of possible coordination modes. In such a ligand, reports have appeared showing that the ligating centers may collectively bind to one metal, such as in the helical pt-quinquepyridine Co(II) complex reported[9] earlier in our study. It may also bind in a pentacoordinate fashion[10a] with Ag(I), or it may behave as terpyridine and bipyridine subunits in the formation of bimetallic, double-stranded helicates.[10b] For the inclusion of three Cu(I) cations, the ligand may divide into smaller segments to accommodate the lower coordination numbers 2 or 3, and there has been no report of this behavior. The coordination number 2 follows from our recent study of Cu(I) terpyridine dimers and the characterization of an air-stable, double-stranded helicate from 6,6″-diphenyl-4,4″-bis(methylthio)-2,2′:6′,2″-terpyridine.[11] X-ray data showed the two Cu(I) centers in tetrahedral and linear coordination environments (coordination numbers 4 and 2), respectively. In solution, NMR data established that the complex assumed a more symmetrical geometry with retention of the double-stranded helicate structure, and significant metal–metal interaction was observed with $\Delta E^{\circ\prime} = 860$ mV. Following the two-dimensional representation used in part 1 of this series, and reasoning by analogy, Scheme I shows possible solid-state tetrahedral/linear coordination geometries anticipated for a series of Cu(I) double-stranded helicates from the odd-numbered oligopyridines, terpyridine through novipyridine. We were specifically interested in the trends affecting stability and the interrelationships of these diverse double-stranded helicates, in their potential for metal–metal interaction, and in establishing the intramolecular electron transfer in mixed-valence systems which has not been observed in these systems.

Scheme I. Possible Tetrahedral/Linear Coordination Patterns of Odd-Numbered Oligopyridines with Cu(I) Cations in the Solid State

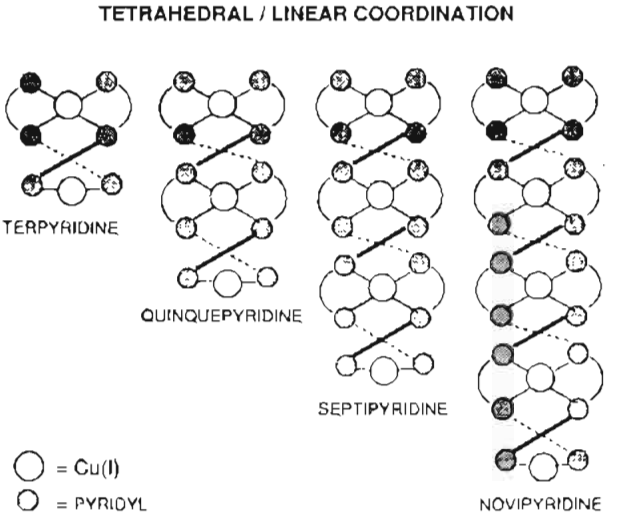

Experimental Section

Electrochemical and spectroscopic measurements were performed in acetonitrile, *N,N*-dimethylformamide (DMF), dimethyl sulfoxide (DMSO) (all Burdick and Jackson distilled in glass, dried over 4-Å molecular sieves), CH_2Cl_2 (Fisher, distilled from P_2O_5), or CH_3NO_2 (Aldrich, distilled from CaH_2). The supporting electrolytes were either tetrabutylammonium perchlorate (TBAP) (GFS Chemicals), which was recrystallized three times from EtOAc and dried under vacuum for 72 h, or tetrabutylammonium hexafluorophosphate, prepared from tetrabutylammonium bromide and hexafluorophosphoric acid, followed by recrystallization from EtOAc. Supporting electrolyte concentrations were 0.1 M unless otherwise indicated. All electrochemical experiments were performed using a platinum disk electrode ($A = 0.08$ cm^2), which was polished prior to use with 1-μm diamond paste (Buehler) and rinsed thoroughly with water and acetone. A saturated sodium calomel electrode (SSCE) was used as reference without regard for the liquid-junction potential. A coiled platinum wire formed the counter electrode, and electrochemical cells were of conventional design. Solutions for electrochemistry were typically millimolar in the redox species and were deoxygenated by purging with prepurified nitrogen for at least 10 min. Unless otherwise stated, the sweep rate in cyclic voltammetric experiments was 100 mV/s.

The electrochemical instrumentation utilized was a Pine Instrument Co. Model RDE3 electrochemical analyzer, and data were recorded on a Soltec Model VP-6423S recorder. Ultraviolet–visible spectra were obtained using a Hewlett Packard 8451A diode array spectrophotometer in conventional 1-cm quartz cells. Spectroelectrochemical experiments were carried out in a three-compartment (separated by medium-porosity glass frits) Pyrex cell with the central compartment placed in the light path of the spectrophotometer. The working electrode was a 0.5-cm^2 piece of Pt gauze (52 mesh, Aldrich), and electrical contact was made through a Pt wire spot welded to the Pt gauze. The counter and reference electrodes used for these experiments were as described above. Fast-scan cyclic voltammograms were obtained using a Pt microelectrode ($r = 22$ μm).

Mass spectral data were obtained on a Kratos MS-890 or a VG ZAB-SE spectrometer with 3-nitrobenzyl alcohol as matrix, either at Cornell University or the University of Illinois. ^{1}H NMR spectra were determined on a Varian 500-MHz NMR spectrometer using TMS as internal standard. FT-IR measurements were made on a Perkin-Elmer FT-IR near-IR spectrophotometer, and combustion analyses were performed by Quantitative Technologies, Inc., Whitehouse, NJ. Magnetic moment

(6) (a) Constable, E. C.; Elder, S. M.; Healy, J.; Tocher, D. A. *J. Chem. Soc., Dalton Trans.* **1990**, 1669. (b) Constable, E. C.; Elder, S. M.; Healy, J.; Ward, M. D. *J. Am. Chem. Soc.* **1990**, *112*, 4590.

(7) (a) Lehn, J.-M.; Sauvage, J.-P.; Simon, J.; Ziessel, R.; Piccinni-Leopardi, C.; Germain, G.; Declercq, J.-P.; Van Meerssche, M. *Nouv. J. Chim.* **1983**, *7*, 413. (b) Gisselbrecht, J.-P.; Gross, M.; Lehn, J.-P.; Sauvage, J.-P.; Ziessel, R.; Piccinni-Leopardi, C.; Arrieta, J. M.; Germain, G.; Van Meerssche, M. *Nouv. J. Chim.* **1984**, *8*, 661. (c) Lehn, J.-M.; Rigault, A.; Siegel, J.; Harrowfield, J.; Chevrier, B.; Moras, D. *Proc. Natl. Acad. Sci. U.S.A.* **1987**, *84*, 2565.

(8) Constable, E. C.; Hannon, M. J.; Martin, A.; Raithby, P. R.; Tocher, D. A. *Polyhedron* **1992**, *11*, 2967.

(9) Gheysen, K. A.; Potts, K. T.; Hurrell, H. C.; Abruña, H. D. *Inorg. Chem.* **1990**, *29*, 1589.

(10) (a) Constable, E. C.; Drew, M. G. B.; Forsyth, G.; Ward, M. D. *J. Chem. Soc., Chem. Commun.* **1988**, 1450. (b) Constable, E. C.; Elder, S. M.; Raithby, P. R.; Ward, M. D. *Polyhedron* **1991**, 1395 and earlier references listed therein.

(11) Potts, K. T.; Keshavarz-K, M.; Tham, F. S.; Abruña, H. D.; Arana, C. *Inorg. Chem.*, in press.

measurements were made using the NMR method of Evans[12a] in CH_3CN/TMS (10% solution) at 293 K.

Preparation of $[Cu^{I}(mt\text{-}qtpy)]_2[PF_6]_2$ (2b). 4′,4″-Bis(methylthio)-2,2′:6′,2″:6″,2‴-quaterpyridine[1b] (mt-qtpy) (**1b**) (100 mg, 2.48×10^{-4} mol) was added to a colorless solution of $[Cu(CH_3CN)_4][PF_6]$[12b] (92 mg, 2.50×10^{-4} mol) in CH_3CN (10 mL) under N_2 atmosphere. After being stirred for 1 h at room temperature, the resultant black solution was treated with Et_2O (10 mL) and, after a few minutes, black crystals separated. Filtered under a N_2 umbrella, the black crystals were collected (137 mg, 90% yield) and dried. Recrystallization from CH_3CN:Et_2O in a N_2 atmosphere gave dark-red prisms of the complex **2b**: mp > 300 °C; FAB mass spectrum *m/z* (% relative intensity) 1077.5 (5) $[M^+ - PF_6]$, 932.2 (3) $[M^+ - 2PF_6]$, 465.1 (53) $[Cu(mt\text{-}qtpy)^+]$. Anal. Calcd for $C_{44}H_{36}Cu_2F_{12}N_8P_2S_4 \cdot H_2O$: C, 42.62; H, 3.09; N, 9.03. Found: C, 42.54; H, 2.89; N, 8.96.

Preparation of $[Cu^{II}(mt\text{-}qtpy)(CH_3OH)][PF_6]$ (3b). The ligand mt-qtpy (**1b**) (200 mg, 4.90×10^{-4} mol) was added to a solution of $Cu(OAc)_2 \cdot H_2O$ (97 mg, 4.90×10^{-4} mol) in CH_3OH (15 mL). After being stirred for 2 h at room temperature, the resultant dark-blue solution was treated with a saturated, methanolic solution of NH_4PF_6 (200 mg). The indigo-colored salt that separated was collected (344 mg, 99%), washed with H_2O, CH_3OH, and Et_2O, and recrystallized from CH_3CN:Et_2O, from which **3b** separated as indigo-colored, irregular prisms: 310 mg (92%); mp > 300 °C; FAB mass spectrum *m/z* (% relative intensity) 610.46 (34) $[M^+ - PF_6 - CH_3OH]$, 465.0 (52) $[M^+ - 2PF_6 - CH_3OH]$. Anal. Calcd for $C_{22}H_{18}CuF_{12}N_4P_2S_2 \cdot CH_3OH \cdot {}^2/_3CH_3CN$: C, 35.84; H, 2.95; N, 8.02. Found: C, 36.22; H, 2.48; N, 7.40.

Preparation of $[Cu^{II}_2(mt\text{-}qnpy)_2OAc][PF_6]_3$ (5). 4′,4‴-Bis(methylthio)-2,2′:6′,2″:6″,2‴:6‴,2⁗-quinquepyridine[13] (mt-qnpy) (**4a**) (200 mg, 4.17 $\times 10^{-4}$ mol) was added to a solution of $Cu(OAc)_2 \cdot 4H_2O$ (103 mg, 4.17 $\times 10^{-4}$ mol) in CH_3OH (20 mL). After being stirred for 3 h at room temperature, the pale-green solution was treated with a saturated methanolic solution of NH_4PF_6 (200 mg). The resultant pale-green salt was filtered out and washed with methanol. Recrystallization from CH_3NO_2:Et_2O produced dark-green microneedles: 325 mg (100%); mp > 300 °C; FAB mass spectrum *m/z* (% relative intensity) 1376.3 (10) $[M^+ - PF_6 - CH_3COO]$, 1231.5 (22) $[M^+ - 2PF_6 - CH_3COO]$, 1087.1(4) $[M^+ - 3PF_6 - CH_3COO]$, 542.3 $[Cu(mt\text{-}qnpy)^+]$; magnetic moment 5.76 μ_B. Anal. Calcd for $C_{56}H_{45}Cu_2F_{18}N_{10}O_2P_3S_4$: C, 42.57; H, 2.87; N, 8.86. Found: C, 42.55; H, 3.01; N, 8.49.

Preparation of Copper Mandelate. Hydrated $CuCl_2$ (1.34 g, 0.01 mol), dissolved in H_2O (50 mL), was treated with (+)-mandelic acid in excess, and the reaction mixture was stirred at room temperature for 4 h. A pale-blue crystalline product separated, which was collected and air-dried: mp 273–275 °C dec; $[\alpha]_D^{24} = +338°$. Anal. Calcd for $C_{18}H_{14}CuO_6$: C, 52.53; H, 3.86. Found: C, 52.47; H, 3.67.

Preparation of $[Cu^{II}(mt\text{-}qnpy)]_2[PF_6]_4$ (6a). The ligand mt-qnpy (**4a**) (100 mg, 2.01×10^{-4} mol) was added to a solution of the above copper mandelate (73 mg, 2×10^{-4} mol) in CH_3OH (15 mL). After the dark-green reaction mixture was stirred at room temperature for 2 h, it was treated with a saturated methanolic solution of NH_4PF_6 (150 mg). The resultant yellow-green salt was collected and washed with CH_3OH, followed by Et_2O (150 mg, 90%). Recrystallization from CH_3CN:Et_2O afforded pale-green needles: 135 mg (91%); mp > 300 °C; FAB mass spectrum *m/z* (% relative intensity) 1377.2 (4) $[M^+ - 2PF_6]$, 1231.2 (20) $[M^+ - 3PF_6]$, 543 (63) $[Cu(mt\text{-}qnpy)^+]$; magnetic moment 5.64 μ_B. Anal. Calcd for $C_{54}H_{42}Cu_2F_{24}N_{10}P_4S_4 \cdot 2H_2O$: C, 38.11; H, 2.71; N, 8.23. Found: C, 38.29; H, 2.66; N, 7.96.

Preparation of $[Cu^{II}/Cu^{I}(mt\text{-}qnpy)_2][PF_6]_3$ (6b). The ligand mt-qnpy (**4a**) (200 mg, 4.17×10^{-4} mol) was added to a colorless solution of $[Cu(CH_3CN)_4][PF_6]$ (233 mg, 6.3×10^{-4} mol) in CH_3CN (20 mL). The formation of an immediate brown solution marked complex formation. After stirring of the reaction solution at room temperature for 2 h, the brown complex was exposed to air, and the product was precipitated by the addition of Et_2O, collected, washed with CH_3CN:Et_2O (1:1), and air dried (305 mg, 96%). It crystallized from CH_3NO_2:Et_2O as dark-red prisms: 280 mg (88%); FAB mass spectrum *m/z* (% relative intensity) 1231.3 (7) $[M^+ - 2PF_6]$, 1084.1 (1) $[M^+ - 3PF_6]$, 541.8 (16) $[Cu(mt\text{-}qnpy)^+]$. Anal. Calcd for $C_{54}H_{42}Cu_2F_{18}N_{10}P_3S_4 \cdot 4H_2O$: C, 40.67; H, 3.13; N, 8.79. Found: C, 40.70; H, 2.87; N, 8.99.

Preparation of $[Cu^{I}_3(mt\text{-}qnpy)_2][PF_6]_3$ (7). The ligand mt-qnpy (**4a**) (100 mg, 2.1×10^{-4} mol) was added to a colorless solution of $[Cu(CH_3CN)_4][PF_6]$ (155 mg, 4.17×10^{-4} mol) in deoxygenated CH_3OH (20 mL), the reaction system being under a dry N_2 atmosphere. The initial colorless solution immediately changed to a dark-brown color, indicative of complex formation. After stirring of this brown reaction mixture for 3 h at room temperature, the separated brown product was collected and washed with CH_3OH under a N_2 atmosphere and dried in a vacuum desiccator: 167 mg (100%); FAB mass spectrum *m/z* (% relative intensity) 1376 (8) $[M^+ - Cu - PF_6]$, 1231.1 (62) $[M^+ - Cu - 2PF_6]$, 1086.1 (29) $[M^+ - Cu - 3PF_6]$. Anal. Calcd for $C_{54}H_{42}Cu_3F_{18}N_{10}P_3S_4$: C, 40.92; H, 2.67; N, 8.84. Found: C, 40.60; H, 2.68; N, 8.59.

Similarly the ligand **4b** gave $[Cu^{I}_3(pt\text{-}qnpy)_2][PF_6]_3$ as a brown powder (quantitative yield) isolated as above: mp > 300 °C; ^1H NMR (acetone-d_6, 500 MHz) δ 8.28 (dd, 4, arom), 8.14–8.01 (m, 18, arom), 7.86 (bd, 4, arom), 7.34 (bs, 4, arom), 3.48 (m, 8, $SCH_2CH_2CH_3$), 1.96 (m, 8, $SCH_2CH_2CH_3$), 1.21 (t, 12, $SCH_2CH_2CH_3$); FAB mass spectrum *m/z* (% relative intensity) 1488.4 (2.2) $[M^+ - Cu - PF_6]$; 1343.8 (13.6) $[M^+ - Cu - 2(PF_6)]$; 1198.8 (3.7) $[M^+ - Cu - 3PF_6]$. Anal. Calcd for $C_{62}H_{58}Cu_3F_{18}N_{10}P_3S_4$: C, 43.88; H, 3.45; N, 8.25. Found: C, 44.16; H, 3.43; N, 8.26.

X-ray Structural Determinations. Crystal selection and mounting were done in a cold room (2 °C) to avoid loss of solvent of crystallization, which caused marked deterioration of the crystal. After the selected crystal was dipped into epoxy resin, it was attached onto a glass fiber before the epoxy hardened, and after being set aside for 1 h, the crystal was mounted on a goniometer head. Siemens standard procedures and programs were used for all operations.

Crystal Data for 2b: $C_{44}H_{36}Cu_2N_8S_4(PF_6)_2 \cdot 2CH_3CN$, monoclinic dark-red prism of 0.26 × 0.28 × 0.37 mm, prepared by slow diffusion of Et_2O into a wet CH_3CN solution of **2b**, M = 1304.2, space group *I*2/*a* (No. 15), a = 17.021(4) Å, b = 16.212(4) Å, c = 20.30(4) Å, β = 103.09(2)°, V = 5457(2) Å^3, Z = 4, and D_c = 1.588 Mg m^{-3}. Data were collected at room temperature (21 °C) using a Siemens R3m diffractometer with Cu Kα radiation (graphite monochromator; λ = 1.541 78 Å) in a Wyckoff scan mode ($\omega = 1.30° + [2\theta(K\alpha_1) - 2\theta(K\alpha_2)]$; 2θ range = 3–115°). The reflections were measured with a variable scan speed (5.00–29.30°/min) and an ω scan range of 1.30°, four check reflections being measured for every 60 reflections in a total of 8078 reflections collected of which 3131 were uniquely observed ($F > 4.0\sigma F$). Lorentz, polarization, and semiempirical absorption corrections were applied [μ(Cu) = 3.71 mm^{-1}]. Siemens programs, SHELXTL PLUS (release 4.21/V), were used for phase determinations and structure refinements. Systematically absent reflections indicated two possible space groups, *I*2/*a* (No. 15) and *Ia* (No. 9). The distribution of intensities ($E^2 - 1$ = 0.996) indicated a centrosymmetric space group, *I*2/*a* (No. 15), and the data were refined using this space group. The positions of the Cu atoms were identified in a Patterson vector map, and direct methods of phase determination led to an electron-density map from which the non-hydrogen atoms were identified, except the molecule of acetonitrile of crystallization. The Cu cation complex was located on a 2-fold rotation axis parallel to the *b*-axis. Subsequent isotropic refinement led to the identification of a molecule of acetonitrile in the asymmetric unit. Disorder existed in the hexafluorophosphate anion, the population ratio being 68%:32%, and the phosphorous–fluorine distances were constrained to 1.560(9) Å during least-squares refinement. Atomic coordinates and isotropic and anisotropic temperature factors of all non-hydrogen atoms were refined by means of a full-matrix least-squares procedure. The methyl hydrogens on one of the methylthio groups were present in two conformations, population ratio 85%:15%. All hydrogen atoms were included in the refinement in calculated positions riding on the atoms to which they are attached and with fixed isotropic temperature factors. The refinement converged at R = 4.61% and R_w = 7.72%. The background in the electron density map was 0.36 e/Å^3.

Crystal Data for 5: $C_{56}H_{45}Cu_2N_{10}O_2S_4(PF_6)_3 \cdot 6H_2O$, orthorhombic green prism of 0.40 × 0.44 × 0.52 mm, prepared from a CH_3CN solution of **5** by the slow diffusion of Et_2O, M = 1688.4, space group *Pbnn* (No. 52), a = 16.558(3) Å, b = 16.684(3) , c = 25.577(4) Å, $\alpha = \beta = \gamma$ = 90°, V = 7066(2) Å^3, Z = 4, and D_c = 1.587 Mg m^{-3}. Using the procedures described for **2b** [with the following parameters: ω scan range = 2.00°; 2θ = 3–115°; variable scan speed = 3.00–29.30°/min; μ(Cu) = 3.43 mm^{-1}; 5303 reflections collected, 3180 unique reflections ($F > 4.0\sigma F$)], the two Cu atoms were found to be located in special positions along the 2-fold rotation axis parallel to the *b*-axis. One phosphorous atom of the hexafluorophosphate anions was located on an inversion center, and two carbon atoms of the acetate group were also located on the 2-fold axis

(12) (a) Evans, D. F. *J. Chem. Soc.* **1959**, 2002. (b) Kubas, G. J. *Inorg. Synth.* **1979**, *14*, 90.
(13) Potts, K. T.; Cipullo, M. J.; Ralli, P.; Theodoridis, G. *J. Org. Chem.* **1982**, *47*, 3027.

passing through the Cu atoms. Subsequent isotropic refinement led to the identification of four molecules of water in the asymmetric unit, where two oxygen atoms were located on the 2-fold rotation axis parallel to the *a*-axis. The oxygen atoms of these four molecules of water had relatively high thermal motions. Because the acetate carbons were located on a 2-fold rotation axis, the methyl hydrogens of the group were inherently present in two conformations, with 50% site occupancy for each conformation. The refinement converged at $R = 8.24\%$ and $R_w = 12.64\%$. The background in the electron-density map was 0.79 e/Å^3.

Crystal Data for 6b: $C_{54}H_{42}N_{10}S_4Cu_2(PF_6)_3 \cdot 3.208CH_3NO_2$, monoclinic dark-red prism of 0.18 × 0.28 × 0.44 mm, prepared from a CH_3NO_2 solution of **6b** by the slow diffusion of Et_2O, M = 1710.0, space group *I*2/*a* (No. 15), a = 25.002(6) Å, b = 15.501(4) Å, c = 33.560(6) Å, β = 91.09(2)°, V = 13004(4) Å^3, Z = 8, and D_c = 1.754 Mg m^{-3}. Using the procedures described for **2b** [with the following parameters: ω scan range = 1.20°; 2θ = 3–115°; variable scan speed = 3.00–29.30°/min; μ(Cu) = 3.79 mm^{-1}; 20 919 reflections collected, 6172 unique reflections ($F > 4.0\sigma F$)], systematically absent reflections indicated two possible space groups, *I*2/*a* (No. 15) and *Ia* (No. 9). The distribution of intensities ($E^2 - 1 = 0.980$) indicated a centrosymmetric space group *I*2/*a* (No. 15), and the data were refined using this space group. The positions of the two Cu atoms were identified in a Patterson vector map. Direct methods of phase determination led to an electron density map from which the non-hydrogen atoms were identified, except for the four molecules of nitromethane of crystallization, which were identified on subsequent isotropic refinement. The sites of three of these four nitromethane molecules were partially occupied (84, 79, and 60%), and during the least-squares refinement the C–N and N–O bond distances of these three partially occupied nitromethane molecules were constrained to 1.362(14) and 1.178(12) Å, respectively. One of the three PF_6^- anions was located on a 2-fold rotation axis, parallel to the *b*-axis, this axis passing through the phosphorous and two fluorine atoms. There were two sets of fluorine atoms in this anion with a site population of 65%:35%. Atomic coordinates, isotropic and anisotropic temperature factors of all non-hydrogen atoms were refined by means of blocked full-matrix least-squares procedures. All hydrogen atoms were included in the refinement in calculated positions riding on the atoms to which they were attached and with fixed isotropic temperature factors, the refinement converging at $R = 5.99\%$ and $R_w = 7.57\%$. The background in the electron-density map was 0.34 e/Å^3.

Results and Discussion

Functionalized Quaterpyridines. (a) Bimetallic Helicates with Distorted Tetrahedral Coordination Geometry. 4′,4″-Bis(methylthio)-2,2′:6′,2″:6″,2‴-quaterpyridine (mt-qtpy) (**1b**) can accommodate all the possible modes of coordination (lack of preorganization) anticipated for a tetradentate ligand. In acetonitrile solution it reacted immediately with $[(CH_3CN)_4Cu^I][PF_6]$, giving in quantitative yield the red-black complex $[Cu^I(mt\text{-}qtpy)]_2[PF_6]_2$ (**2b**), precipitated from solution with diethyl ether. Its molecular formula, $C_{44}H_{36}Cu_2F_{12}N_8P_2S_4$, was established from a combination of mass spectral (FAB) data and combustion elemental analysis. The molecular ion at m/z 1077.5 (5%) corresponded to $[M^+ - PF_6]$, and fragment ions consistent with this molecular composition are listed in the Experimental Section.

The tetrahedral-like coordination geometry of the double-stranded helical complex is clear from the single-crystal X-ray structure (Figure 1; structural parameters Table I). The two strands of the ligand each form half a pitch (7.6 Å) of a double helix with a full pitch of approximately 15.2 Å. The diameter of the circumscribed cylinder, measured from sulfur to sulfur atom on two different strands, is 12.39 Å, whereas from carbon to carbon it is 9.28 Å. The complex is located on a unique, 2-fold rotating axis of symmetry parallel to the *b*-axis of the unit cell. This axis (labeled *B* in Figure 1A) is a perpendicular bisector of the Cu(1)–Cu(2) axis (labeled *A* in Figure 1A) and also bisects each of the two bonds joining the two bipy units in each strand of the mt-qtpy ligand. Two additional 2-fold pseudosymmetrical axes (*A* and *C* in Figure 1A) are present and are approximately orthogonal to the above unique 2-fold axis. Of particular interest is the fact that both ligands are located on this 2-fold *B*-axis of the complex. These three rotational axes are also present in solution as determined from the ^{1}H NMR data discussed below. Figure 1A shows the distorted tetrahedral coordination of each copper cation and the dihedral angle of 60.7° between each bipy unit plane of one quaterpyridine strand and an analogous angle of 61.2° in the other strand. The distorted tetrahedron of Cu(1) has angles (deg) as follows: N(1)–Cu(1)–N(2), 80.1(1); N(2)–Cu(1)–N(2A), 133.6(1); N(1A)–Cu(1)–N(2A), 80.1(1); N(1)–Cu(1)–N(1A), 140.7(1); N(2)–Cu(1)–N(1A), 115.3(1); N(1)–Cu(1)–N(2A), 116.5(1). The dihedral angle about the planes Cu(1)–N(1)–N(1A), Cu(1)–N(2)–N(2A) defined by a Cu cation is 110.7° (or acute angle of 69.3° given in Table 1), and the dihedral angles between the planes of each pyridine ring in a bipy unit are 8.0° (1st strand) and 7.3° (2nd strand). The average π–π-stacking distance between adjacent (parallel) strands of the ligand is 3.45 Å, and the nonbonded distance Cu(1)···Cu(2) is 3.32 Å (see Figure 1A). The helical complex crystallizes in a centrosymmetric space group, *I*2/a (No. 15). As a consequence, both left-handed (M) and right-handed (P) helices are present in the unit cell. This double-stranded bimetallic helicate is cylindrical (constant radius) and palindromic (constant pitch).

In his initial study in this general area Lehn[7] found that the ligand **1a** with partial preorganization formed the helicate **2a**, and a comparison of the structural parameters of **2b** with those of **2a** is especially important, particularly in view of their divergent redox chemistry described below. The spatial requirements of the two inner-ring methyl substituents in **2a** affect the general shape of the double helix in several ways. The increase in the dihedral angle between two bipy rings in the same strand from 60.7° (1st strand) and 61.2° (2nd strand) in **2b** to 75 and 77° in **2a** results in an increase in the Cu–Cu distance from 3.32 to 3.90 Å ($\Delta = 0.58$ Å). The methyl substituents also have a marked effect on the symmetry of the complex. The unique 2-fold *B*-axis bisecting each of the two bonds joining the two bipy units in each strand is absent in the complex **2a**. There is also a change in the dihedral angles between two pyridine rings in a bipy unit from 8.0° (1st strand) and 7.3° (2nd strand) in **2b** to 8 and 15°, respectively, in **2a**. Similar changes in the dihedral angles about the planes defined by a copper cation are observed: in **2b** the angle of 110.7° changes to 99 and 97° in **2a**. The ^{1}H NMR spectrum (Figure 2) (500 MHz) for **2b** shows six chemical shifts (Table II) attributable to aromatic protons in each of the four bipy segments (a total of 24 aromatic protons), which are the result of three 2-fold symmetry axes, as well as an SCH_3 substituent in a pyridine 4-position in two of the pyridine rings. In this Cu(I) helicate **2b** there is contraction with an overall upfield shift of the aromatic protons (δ 7.37–8.05, $\Delta\delta = 0.68$) when compared to analogous aromatic protons in the ligand (δ 7.36–8.71, $\Delta\delta = 1.35$). Protons 4 and 5 are shifted downfield, and the rest of the protons are shifted upfield.

(b) Monometallic Tetradentate Complexes. Reaction of bis(methylthio)quaterpyridine (**1b**) and Cu(II) acetate in methanol, followed by counterion exchange with hexafluorophosphate, yielded a monometallic complex $[Cu^{II}(mt\text{-}qtpy)\cdot CH_3OH][PF_6]_2$ (**3b**). In this case mt-qtpy adopts a planar tetradentate mode resulting in a complex with square pyramidal geometry, with solvent (CH_3OH) occupying the apical position, this structural assignment being based on that given[7] to the similar complex **3a**. The relationship of complex **3b** to the double-stranded helical complex **2b** is shown in Scheme II. Chemical reduction of **3b** with hydrazine in CH_3CN, or electrochemical reduction, resulted in the bimetallic complex **2b**. This process was reversible, as air or electrochemical oxidation converted **2b** into **3b**.

Electrochemical Characterization: Mt-quaterpyridine (1b)–Cu Complexes. Electrochemical data for mt-quaterpyridine (**1b**) complexes are presented in Table III. The cyclic voltammograms of $[Cu^{II}(mt\text{-}qtpy)\cdot CH_3OH][PF_6]_2$ (**3b**) and $[Cu^I(met\text{-}qtpy)]_2[PF_6]_2$ (**2b**) in 0.1 M TBAP/DMSO solutions are shown in Figures

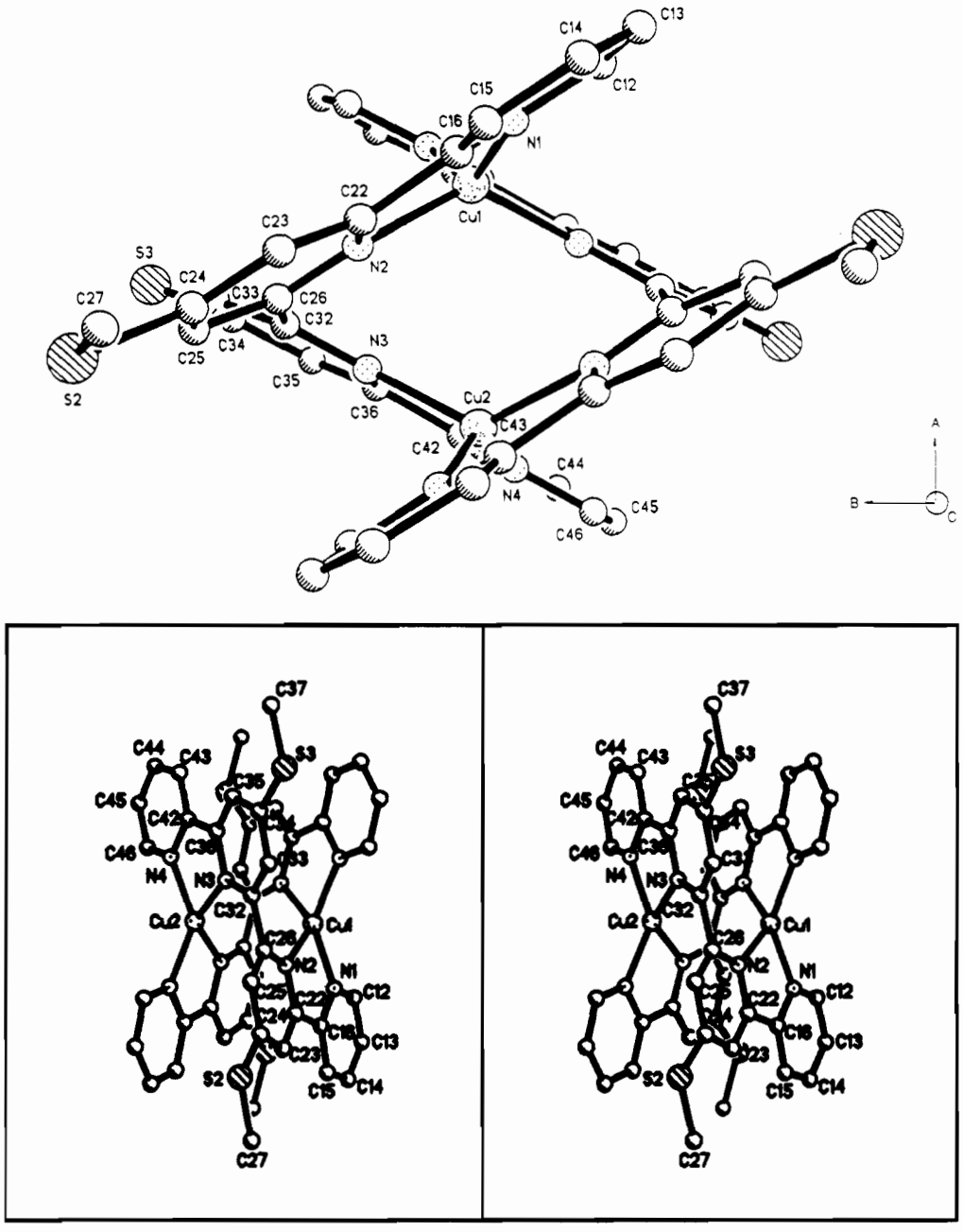

Figure 1. (A) Top: X-ray structure of **2b** (plan view) with *C* axis pointing out of the plane of the paper, showing stacking of bipyridine units in adjacent strands. (B) Bottom: Stereotopic view of the right-handed (P) bimetallic helicate **2b** along the *B*-axis.

3 and 4, respectively. The cyclic voltammogram of the Cu(II) complex (**3b**) showed a one-electron, irreversible reduction at –0.06 V corresponding to a metal-based reduction of the copper center to Cu(I) (Figure 3). Following reduction, the complex rapidly dimerized to form the helicate $[Cu^{I}(mt\text{-}qtpy)]_2^{2+}$ (**2b**), and therefore, upon scan reversal at –0.35 V, no return wave was observed for the reduction at –0.06 V. The generated $[Cu^{I}(mt\text{-}qtpy)]_2^{2+}$ (**2b**) underwent a two-electron process at +0.38 V in which both copper centers were oxidized to Cu(II). The oxidized dimer rapidly reorganized to generate the monometallic complex **3b**. The lack of a return wave at +0.38 V and the appearance of the reduction wave for the monometallic complex at –0.06 V support these transformations. Additional evidence comes from the fact that if, on a negative going sweep, the scan direction were reversed prior to the reduction at –0.06 V, the oxidative wave at +0.38 V was completely absent, thus establishing that this process originated from the reduction at –0.06 V.

These processes are further corroborated by the voltammetric response of a solution of a known sample of the bimetallic complex $[Cu^{I}(mt\text{-}qtpy)]_2[PF_6]_2$ (**2b**) (Figure 4). In this case, the voltammetric scan was started at –0.35 V and, upon scanning positively, a two-electron oxidation was observed at +0.38 V. This wave corresponded to the oxidation of both copper centers to Cu(II) and was observed at the same potential where the electrogenerated dimer oxidized. Upon scan reversal at +0.60 V, the one-electron reduction of the electrogenerated monometallic complex occurred at –0.08 V. These transformations are described by the redox processes shown in Scheme III.

The fast-scan cyclic voltammogram (Figure 5) for a solution of $[Cu^{II}(mt\text{-}qtpy)\cdot CH_3OH][PF_6]_2$ (**3b**) in 1 M TBAP/DMSO at a Pt microelectrode (r = 22.3 μm) at 4 kV/s provides further support for the redox processes shown in Scheme III. At such a fast-scan rate, the redox process at +0.38 V appeared to be quasi-reversible with a formal redox potential of +0.16 V *vs* Ag (+0.18 V *vs* SSCE). However, the peak corresponding to reduction of the Cu(II) monomer appeared chemically irreversible at sweep rates up to 20 kV/s, suggesting that this is a much faster process. A detailed study of these phenomena including results of digital simulations will be described in a later publication.

In the negative potential region, both complexes exhibited

Table I. X-ray Structural Parameters of Bimetallic, Double-Stranded Helical Complexes **2b**, **5**, and **6b**

	complex		
	2b	**5**	**6b**
R (%)	4.61	8.24	5.99
Cu–Cu dist (Å)	3.32	4.44	4.25
pitch height (Å)	7.6	7.9	9.2
helical diameter[a] (Å)			
C_{14}–C_{14a}	9.28		9.14 (tet)
C_{44}–C_{44a}		9.42	9.46 (oct)
S_2–S_{2a}	12.39	12.60	12.04 (tet)
S_4–S_{4a}		12.91	12.88 (oct)
ring Interannular angles (deg) (first strand; second strand)			
1,2; 1A,2A	8.0; 7.3	14.6; 14.6	6.3; 7.0
2,3; 2A, 3A	55.4; 59.7	40.4; 40.4	63.5; 70.1
3,4; 3A,4A	8.0; 7.3	28.2; 28.2	18.7; 5.1
4,5; 4A,5A		2.7; 2.7	2.9; 6.4
dihedral angles (deg) between			
bipy–bipy at Cu_1	69.3	70.3	78.0
terpy–terpy at Cu_2		79.9	82.2
bipy–bipy at Cu_2	69.3		
av π–π stacking dis between py rings (Å) metal–nitrogen bond lengths (first strand) (Å)	3.45	3.41	3.44
N_1–Cu_1	2.020(3)	1.982(7)	2.022(5)
N_2–Cu_1	2.063(3)	2.145(6)	2.031(5)
N_3–Cu_2	2.020(3)	2.349(6)	2.298(5)
N_4–Cu_2	2.063(3)	1.948(6)	1.974(5)
N_5–Cu_2		2.171(7)	2.145(5)
metal–nitrogen bond lengths (second strand) (Å)			
N_{1a}–Cu_1	2.030(3)	1.982(7)	2.009(6)
N_{2a}–Cu_1	2.072(3)	2.145(6)	2.066(5)
N_{3a}–Cu_2	2.030(3)	2.349(6)	2.307(5)
N_{4a}–Cu_2	2.072(3)	1.948(6)	1.973(5)
Na_{5a}–Cu		2.171(7)	2.170(5)
metal–oxygen bond length (Å)			
O_{1a}–Cu_1		2.271(11)	
O_{1aa}–Cu_1		2.271(11)	

[a] Denotes atoms used in diameter measurement.

similar voltammetric responses. The cyclic voltammogram for $[Cu^I(mt\text{-}qtpy)]_2[PF_6]_2$ (**2b**) in 0.1 M TBAP/DMSO in the region between 0.0 and –2.0 V is shown in Figure 6. Four one-electron reductions with formal potentials of –1.38, –1.58, –1.83, and –2.02 V were observed, and all four processes are attributed to ligand-based reductions.

Spectroscopic and Spectroelectrochemical Measurements. The band maxima (λ_{max}) and molar absorptivities (ϵ) obtained from the electronic spectra of these complexes are presented in Table IV. In general, the UV region of the electronic spectra of these complexes was dominated by intense intraligand π–π^* transitions. The transitions observed in the visible region are attributed to MLCT transitions[2a,14] (444 and 550 nm) in Cu(I) complex **2b** and to a weak d–d transition (626 nm) in the Cu(II) complex **3b**. The transformation between the monometallic and bimetallic complex was also studied spectroelectrochemically, where changes in the visible spectrum of the complexes were monitored as a function of the applied potential at a Pt gauze working electrode. Figure 7 shows spectral changes in a solution of $[Cu^{II}(mt\text{-}qtpy)\cdot CH_3OH][PF_6]_2$ (**3b**) as a potential of –0.30 V was applied. The dashed line (lower-most trace) represents the spectrum of $[Cu^{II}(mt\text{-}qtpy)\cdot CH_3OH][PF_6]_2$ before electrolysis in 0.1 M TBAP/acetonitrile. The complex exhibited a broad, weak absorption centered about 610 nm. The solid lines represent the visible spectra obtained every 3 min at an applied potential of –0.30 V. As the solution was electrolyzed, two absorption bands developed at 444 and 520 nm, respectively, these absorptions being characteristic of MLCT transitions in Cu(I) complexes. The energy and shape of these bands are identical to those in the spectrum of $[Cu^I(mt\text{-}qtpy)]_2[PF_6]_2$ (**2b**) and thus lend further support to the dimerization described above. For comparison, the spectrum of a known sample of $[Cu^I(mt\text{-}qtpy)]_2[PF_6]_2$ is also shown in Figure 7 as the top-most trace. The dimerization process was found to be reversible. After 1 h of electrolysis, the applied potential was changed to +0.60 V, and after an additional 1 h of electrolysis, the spectrum of $[Cu^{II}(mt\text{-}qtpy)\cdot CH_3OH][PF_6]_2$ was regenerated.

Spectroelectrochemical measurements on $[Cu^I(mt\text{-}qtpy)]_2[PF_6]_2$ (**2b**) were also consistent with the previously mentioned structural changes. Upon oxidative electrolysis at +0.80 V the spectra changed from one characteristic of **2b** to that of **3b**. Again, these changes were reversible.

A dimerization similar to the one described here was observed previously by Lehn and co-workers.[7] They found that upon reduction of their monomeric $[Cu^{II}(CH_3)_4\text{-}qtpy]^{2+}$ complex (**3a**) prepared from the ligand **1a**, the dimeric complex $[Cu^I(CH_3)_4\text{-}qtpy]_2[PF_6]_2$ (**2a**) formed quickly. In this case, however, once the dimeric complex was formed, it was stable and two, reversible, one-electron, metal-based oxidations were observed with formal potentials of +0.72 and +0.53 V vs SCE, respectively. Oxidation of the dimeric complex by cyclic voltammetry did not lead to the regeneration of the monomeric complex, which is contrary to our observations with $[Cu^I(mt\text{-}qtpy)]_2[PF_6]_2$ (**2b**).

This difference in electrochemical behavior may be rationalized in terms of the tetramethyl substitution (5′,3″-dimethyl substituents in each subunit) in the ligand **1a**. The X-ray structure of $[Cu^{II}(CH_3)_4\text{-}qtpy)]^{2+}$ (**3a**) shows[7] that the pyridine nitrogen atoms are coplanar but the rings themselves all have appreciable twists relative to one another, with the greatest dihedral angle being between the two inner rings due to the steric interactions of the methyl groups. Once the complex is reduced to Cu(I), the metal center is more stable in a tetrahedral configuration and a dimer quickly forms. Once the dimer is formed, however, it is stable upon oxidation, and therefore, the monometallic complex is not formed on oxidation as is clearly evident from their voltammetric data. In contrast, the complex **2b** has no such steric constraints

(14) Day, P.; Sanders, N. J. *J. Chem. Soc. A* **1967**, 1530.

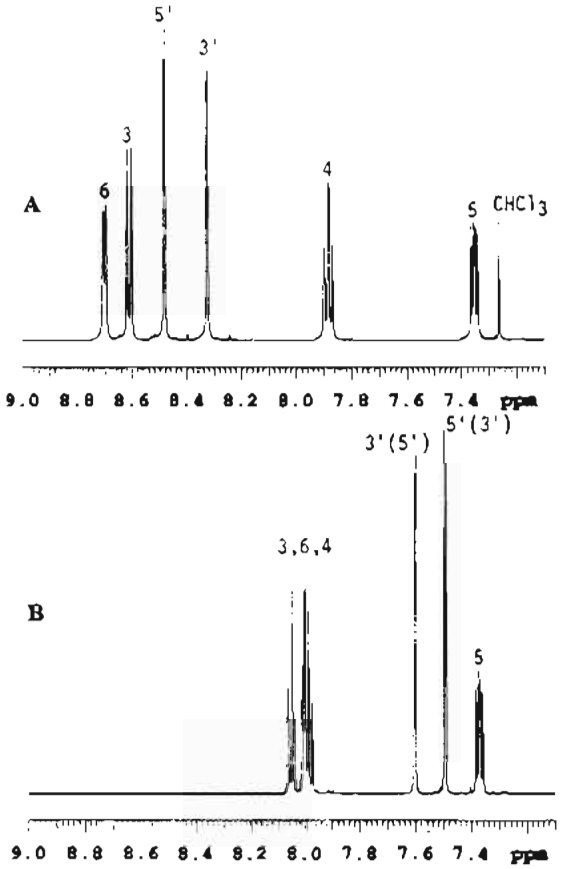

Figure 2. ^{1}H NMR spectra (500 MHz) of (A) the ligand **1b** ($CDCl_3$) and (B) the Cu(I) complex **2b** (CD_3CN).

Table II. Chemical Shifts (δ) and Coupling Constants (Hz) of the Aromatic Protons in the Quaterpyridine Ligand **1b** and its Cu(I) Complex **2b**[a]

compd no.	protons					
	H6	H5	H4	H3	H3′	H5′
2b	8.00	7.37	7.98	8.05	7.60	7.49
	$J_{5,6}$=5.1	$J_{6,5}$=5.1	$J_{3,4}$=8.0	$J_{4,3}$=8.0	$J_{5',3'}$=1.5	$J_{3',5'}$=1.5
	$J_{4,6}$=1.8	$J_{4,5}$=8.0	$J_{5,4}$=8.0	$J_{5,3}$=1.0		
		$J_{3,5}$=1.0	$J_{6,4}$=1.8			
1b	8.71	7.36	7.89	8.64	8.34	8.50
	$J_{5,6}$=4.8	$J_{6,5}$=4.8	$J_{3,4}$=7.8	$J_{4,3}$=7.8	$J_{5',3'}$=1.8	$J_{3',5'}$=1.8
	$J_{4,6}$=1.8	$J_{4,5}$=7.8	$J_{5,4}$=7.8	$J_{5,3}$=1.1		
	$J_{3,6}$=0.8	$J_{3,5}$=1.1	$J_{6,4}$=1.8			

[a] SCH_3 chemical shifts: complex **2b**, δ = 2.70; ligand **1b**, δ = 2.59.

and its electrochemical behavior is governed more by electronic effects resulting from changes in the oxidation states of the metal centers.

It is also of interest to compare our results described above, as well as those of Lehn, with those of Constable and co-workers[8] on the copper complexes of unsubstituted quaterpyridine (**2c**, **3c**). Although very limited electrochemical data is provided in their study, they state that in cyclic voltammetric studies (in acetonitrile/$TBABF_4$) they only observed two irreversible processes at +0.05 and −0.42 V (vs ferrocene/ferrocenium), which would correspond to approximately +0.50 and +0.08 V vs SCE. They ascribe this instability to the closer contact of the copper centers in their complex (Cu–Cu = 3.17 Å) relative to that in the complex prepared by Lehn and co-workers, (Cu–Cu = 3.90 Å). However, it is not clear why a shorter Cu–Cu bond distance should result in the aforementioned instability. We were surprised by the large difference in formal potentials for the redox processes that we observe relative to those reported by Lehn. It is possible that such a shift might be due to stronger interactions by the solvent (acetonitrile) with the metal centers giving rise to a shift

Scheme II. Inter-Relationships between Monometallic Complexes and Bimetallic Double-Stranded Helical Complexes of 4′,4″-Bis(methylthio)-2,2′:6′,2″:6″,2‴-quaterpyridine (**1b**)

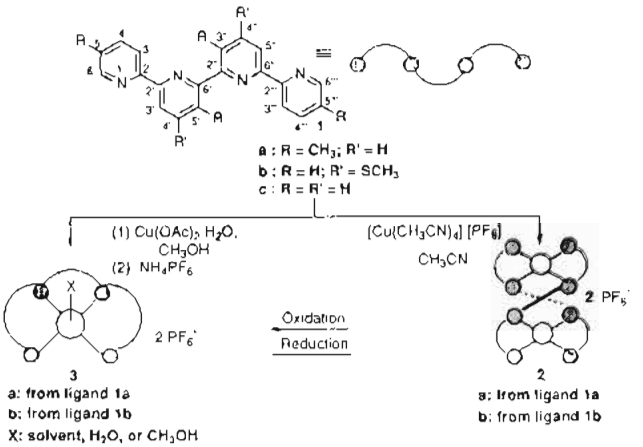

Scheme III. Redox Processes of $[Cu^I(mt\text{-}qtpy)]_2[PF_6]_2$ (**2b**)

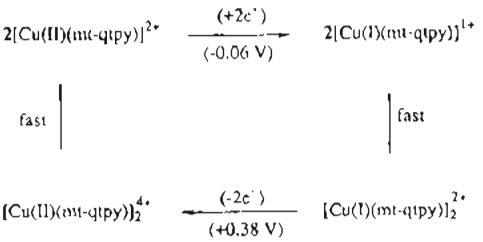

in the oxidation potentials to more positive values. However, we have no direct evidence for this.

The difference in electrochemical behavior that we observe, relative to that reported by Constable and co-workers,[8] is likely due to electronic effects. We have found that the presence of methylthio substituents on terpyridine causes a negative shift of about 60–100 mV in the redox behavior of the Co, Ni, and Fe complexes relative to those of the unsubstituted terpy.[15] If a similar effect were present in the quaterpyridine complexes, then this could account for the previously mentioned differences. However, due to the very limited electrochemical data presented by Constable, a more thorough comparison is not possible at this time.

What is clear, however, is that seemingly subtle differences in the ligands can have rather dramatic effects on the redox behavior of these complexes and point to the overall control that may be achieved in double-stranded, polymetallic helicates of this type by substituent variations.

Functionalized Quinquepyridines. (a) Bi- and Trimetallic Helicates. The physical characteristics of alkylthio-substituted quinquepyridines (mt- or pt-qnpy) (mt = methylthio, pt = *n*-propylthio) make them ideally suited for metal ion-induced self-organization at ambient temperatures. Our work leading to a rich and diverse group of double-stranded helicates containing copper is summarized in Scheme IV.

The ligand **4a** and copper(II) acetate in methanol at room temperature gave the double-stranded helicate **5**, isolated as its hexafluorophosphate salt. The dimeric nature of the complex was initially established by analytical and FAB mass spectral data (Experimental Section), and its double-stranded helical structure was verified by the single-crystal X-ray shown in Figure

(15) Redox potentials (V) vs SCCE in CH_3CN/0.1 M TBAP for metal-based oxidations of Co, Fe, and Ni complexes of terpyridine (tpy) and (methylthio)terpyridine (mt-tpy): $[Co(tpy)_2]^{2+}$, +0.27; $[Co(mt\text{-}tpy)_2]^{2+}$, +0.21; $[Fe(tpy)_2]^{2+}$, +1.10; $[Fe(mt\text{-}tpy)_2]^{2+}$, +1.03; $[Ni(tpy)_2]^{2+}$, +1.55; $[Ni(mt\text{-}tpy)_2]^{2+}$ +1.65. Arana, C. R.; Abruña, H. D.; Potts, K. T.; Keshavarz-K, M. Unpublished results.

Table III. Redox Potentials vs SSCE for Cu Complexes of mt-Quaterpyridine and mt-Quinquepyridine[a]

complex no.	solvent	$E^{\circ\prime}$ (V) [ΔEp (mV)]
3b	DMSO	+0.38 [irrev], −0.06 [irrev], −1.43 [60], −1.63 [60], −1.86 [80]
2b	DMF	+0.38 [irrev], −0.08 [irrev], −1.38 [70], −1.58 [70], −1.83 [80], −2.02 [90]
5	CH_3CN	+0.48 [70], −0.05 [70], −1.53 [80], −1.72 [90], −1.99 (2e⁻) [60]
	DMF	+0.49 [60], −0.02 [60], −1.53 [80], −1.72 [70], −1.99 (2e⁻) [60]
6a	CH_3CN	+0.48 [60], −0.04 [70], −1.39 [60], −1.74 [80]
	DMF	+0.75 [60], +0.03 [60], −1.39 [80], −1.61 [80]
	DMSO	+0.41 [70], 0.00 [70], −1.44 [60], −1.63 [70], −1.85 [100]
6b	CH_3CN	+0.48 [80], −0.08 [70]
	DMSO	+0.34 [60], −0.01 [60], −1.44 [60], −1.62 [60], −1.88 (2e) [60]
7	CH_3CN	+1.03 [70], +0.50 [50], −0.04 [60], −1.36 [60], −1.61 [60], −1.87 [90], −2.03 [90]

[a] Processes are one-electron transfers except where noted.

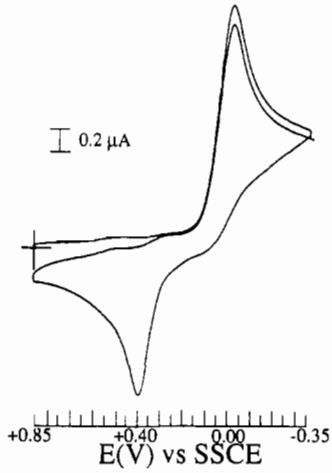

Figure 3. Cyclic voltammogram for $[Cu^{II}(mt\text{-}qtpy)CH_3OH][PF_6]_2$ (**3b**) in 0.1 M TBAP/DMSO.

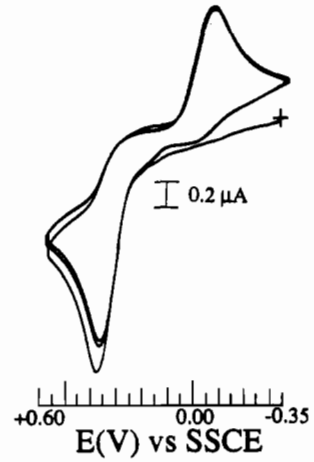

Figure 4. Cyclic voltammogram for $[Cu^{I}(mt\text{-}qtpy)]_2[PF_6]_2$ (**2b**) in 0.1 M TBAP/DMSO.

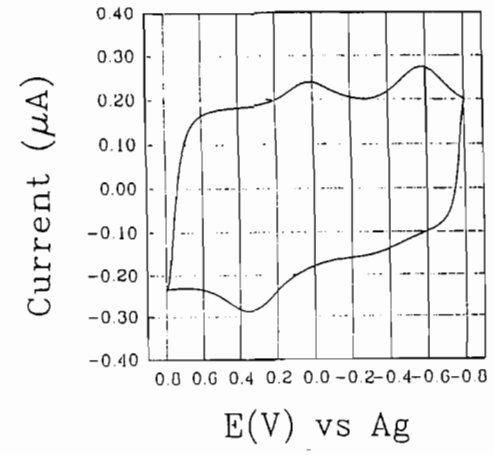

Figure 5. Fast scan cyclic voltammogram at a Pt microelectrode (r = 22.3 μm) at 4 kV/s for a solution of $[Cu^{II}(mt\text{-}qtpy)CH_3OH][PF_6]_2$ (**3b**).

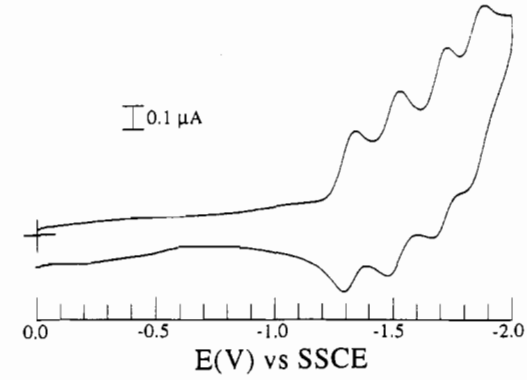

Figure 6. Cyclic voltammogram at negative potentials for $[Cu^{I}(mt\text{-}qtpy)]_2[PF_6]_2$ (**2b**) in 0.1 M TBAP/DMSO.

8. Both copper cations were in a distorted octahedral environment (N_4O_2 and N_6), with an acetate anion completing the coordination sphere of the first Cu atom. It has been reported[16] that ligand **4c** with Cu(II) acetate gave a complex mixture containing helical complexes similar to **5**, **6a**, and **6b**, and these authors separated two Cu(II) complexes by hand from the mixture of crystals obtained. The X-ray structure of their $[L_2Cu^{II}_2OAc][PF_6]$ helicate established its double-stranded helical nature, yet there are subtle but important differences, summarized here, with the data for complex **5** described below. The acetate ion was bonded to the Cu(II) ion in a monodentate fashion, resulting in a very distorted, trigonal bipyramidal geometry. A significant difference, up to 15°, exists in the twist about the C–C interannular bonds in the quinquepyridine strands in this helicate and those observed in **5**. The unique 2-fold rotation axis of **5** which bisects the two Cu atoms lying on the helical axis is absent in their complex and results in the two ligand strands have different structural parameters.

Reaction of **4a** with $[Cu(CH_3CN)_4][PF_6]$ in methanol under a nitrogen atmosphere at ambient temperature resulted in the immediate separation of a brown solid, which, by a combination of analytical and electroanalytical methods (see below), was established as the double-stranded helicate containing three Cu(I) cations and two quinquepyridine strands represented by structure **7**. The ^1H NMR spectrum of the trimetallic Cu(I) complex **7**, obtained from the ligand **4b**, showed a strong complexation effect with an overall contraction and upfield shift of the aromatic protons. This shift of the aromatic protons (Figure 9) is consistent with similar shifts observed in all Cu(I) double-stranded helical complexes derived from terpyridine through octipyridine. The aliphatic region showed only one type of S–CH_2–CH_2–CH_3 group, shifted downfield from that of the

(16) (a) Constable, E. C.; Drew, M. G. B.; Ward, M. D. *J. Chem. Soc., Chem. Commun.* **1987**, 1600. (b) Barley, M.; Constable, E. C.; Corr, S. A.; McQueen, C. S.; Nutkins, J. C.; Ward, D.; Drew, M. G. B. *J. Chem. Soc., Dalton Trans.* **1988**, 2655.

Table IV. Electronic Spectra of Ligands and Complexes (CH_3CN)

complex no.	λ_{max} (nm) (ϵ (cm M)$^{-1}$)
1a	200 (2.86×10^4), 270 (2.22×10^4), 278 (2.31×10^4)
2b	208 (8.53×10^4), 250 (4.66×10^4), 288 (7.04×10^4), 444 (8.67×10^3), 550 (4.94×10^3)
3b	200 (4.49×10^4), 222 (5.95×10^4), 250 sh, 280 sh, 294 (4.42×10^4), 324 (3.53×10^4), 626 (2.70×10^2)
4a	196 (1.20×10^4), 202 (1.57×10^4), 220 (2.14×10^4), 278 (3.86×10^4)
5	200 (2.10×10^5), 226 sh, 250 sh, 292 (7.17×10^4), 475 (1.42×10^2)
6a	200 (1.40×10^5), 296 (1.10×10^5), 330 sh, 670 (3.0×10^2), 1047 (1.73×10^3)
6b	212 (6.54×10^4), 246 (5.34×10^4), 290 (7.01×10^4), 470 (2.86×10^3)
7	196 (1.21×10^5), 286 (8.50×10^4), 434 (4.62×10^3), 550 (2.89×10^3)

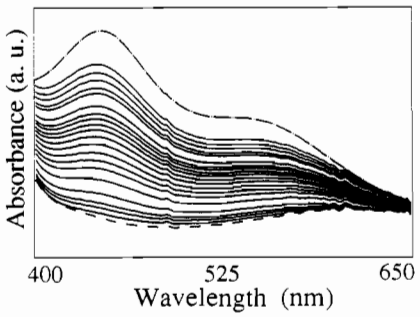

Figure 7. Visible spectra of $[Cu^{II}(mt\text{-}qtpy)CH_3OH][PF_6]_2$ (**3b**) in 0.1 M TBAP/CH_3CN prior to electrolysis (lower-most trace, - - -) and (—) taken every 3 min at an applied potential of –0.30 V, and of $[Cu^{I}(mt\text{-}qtpy)_2][PF_6]_2$ (**2b**) in 0.1 M TBAP/CH_3CN (top-most trace, - - -).

ligand, and a change from an $A_2M_2X_3$ spin system in the ligand[1b] **4b** to an $ABMNX_3$ spin system in complex **7** (Figure 10). The presence of only one type of *S*–*n*-propyl group (out of four possible groups) is due to both a C_2 rotating symmetry axis lying along the helical axis and a C_2 rotating axis bisecting the middle pyridine ring (third ring) in each quinquepyridine strand, suggesting that the complex **7** had adopted a more symmetrical structure than that represented in Scheme IV. The *S*–*n*–propyl substituent is serving as a proton NMR probe in the determination of the helical chirality of the complex **7**. The enantiotopic $-CH_2-$ groups have an A_2 spin system (triplet) in the achiral ligand **4b**, and after complexation, these $-CH_2-$ groups are situated in a chiral environment (helix) and become diastereotopic with an AB spin system (multiplet) (Figure 10C). It is interesting to note that the second $-CH_2-$ group in the *S*–*n*-propyl substituent, in principle a diastereotopic center, also shows a similar change in splitting pattern but in this case the magnitude of the splitting is reduced. These characteristic properties have been utilized and discussed in more detail in our previous publication to demonstrate the solution stability of these Cu(I) and other diamagnetic complexes.[11]

Complex **7** was extremely air-sensitive in solution but stable in the solid state. In solution it was air-oxidized to the bimetallic double-stranded mixed valence complex **6b**, whose X-ray structure is shown in Figure 11 and whose near-infrared spectrum (see below) showed a well-defined intervalence transfer (IT) transition at 1414 nm [ϵ = 70 (cm M)$^{-1}$]. Alternatively, the mixed valence helicate **6b** was prepared directly from **4a** and an acetonitrile solution of $[Cu(CH_3CN)_4][PF_6]$ in the presence of air. Reduction of **6b** with hydrazine or a tertiary amine such as *N*-ethylmorpholine, or by electrochemical methods (see below), resulted in its reorganization to the trimetallic species **7**.

In order to verify the intervalence electron-transfer nature of the absorption in the near-IR region in the mixed-valence helicate **6b**, the homovalence helicate **6a** with an identical coordination geometry was prepared in a unique manner that holds considerable promise for the preparation of similar multimetallic helicates. Thermolysis of the bimetallic helicate **5** to expel the acetate ion was considered too drastic and nonselective for our purposes. Molecular models (CPK models) suggested that if a bulkier Cu(II) carboxylate were used in the self-assembly of **5**, ligand–ligand repulsion would most likely result in expulsion of the carboxylate leading to the bimetallic helicate **6a** with octahedral–tetrahedral coordination geometries. Copper(II) mandelate[17] at room temperature in methanol with **4a** gave the bimetallic helicate **6a** as pale-green needles of its hexafluorophosphate in practically quantitative yield. The two Cu centers with different coordination numbers and geometries have very different absorption bands in the electronic spectrum. An absorption at 670 nm [$\epsilon = 3.0 \times 10^2$ (cm M)$^{-1}$] and one low energy absorption at 1047 nm [$\epsilon = 1.73 \times 10^3$ (cm M)$^{-1}$] were assigned to d–d transitions of distorted octahedral Cu(II) and distorted tetrahedral Cu(II), respectively, by analogy to bis[terpy–Cu(II)] and bis[bipy–Cu(II)] complexes.[18,19] The homovalence helicate **6a** was converted into **5** with ammonium acetate in methanol, and on chemical or electrochemical reduction (see below) it was transformed into the trimetallic helicate **7**.

X-ray Characterization of the Copper Complexes 5 and 6b. The helix in these complexes is generally the result of a series of twists about the C–C interannular bonds in the quinquepyridine strand, the major twist occurring between the second and third rings. This major twist divides the quinquepyridine strand into bipy and terpy segments, and the metal–metal distance in the complex is essentially a function of this dihedral angle. Additional minor twists are present in the bipy and terpy segments resulting in deviations from coplanarity between the individual pyridine rings. This deviation is more pronounced in the Cu(II) complex **5** than in the mixed-valence complex **6b**, which is a conical helix. Table I shows various structural parameters for the two quinquepyridine complexes **5** and **6b**, and these data, together with the structures in Figures 8 and 11, clearly show the effective π–π stackings in both assemblies which are comparable to the π–π stacking in the quaterpyridine complex **2b**.

The Cu(II) complex **5** had the Cu atoms located along the unique 2-fold rotation axis parallel to the *b*-axis of the unit cell. Because of their unique symmetry positions, the first strand of the ligand will generate the second strand of the ligand by this unique 2-fold rotation symmetry operation. Therefore both strands of the ligand will have identical structural parameters as indicated in ring interannular angles and metal–nitrogen bond lengths shown in Table I. The distorted octahedron of Cu(1) has angles (deg) as follows: N(1)–Cu(1)–N(2), 79.1(3); N(2)–Cu(1)–N(2A), 113.6(3); N(2a)–Cu(1)–N(1A), 79.1(3); N(1A)–Cu(1)–O(1A), 83.5(3); O(1A)–Cu(1)–O(1AA), 56.8(5); O(1AA)–Cu(1)–N(1), 83.5(3). The distorted octahedron of Cu(2), however, has angles (deg) as follows: N(3A)–Cu(2)–N(4A), 76.9 (2); N(4A)–Cu(2)–N(5A), 77.3 (2); N(5A)–Cu(2)–N(5), 108.7(4); N(5)–Cu(2)–N(4), 77.3(2); N(4)–Cu(2)–N(3), 76.9(2); N(3)–Cu(2)–N(3A), 97.5(3). The two carbon atoms of the acetate group are also located on the 2-fold axis, and the methyl hydrogens of the acetate group are inherently present in two conformations with 50% site occupancy for each conformation.

(17) We prepared optically active copper (+)-mandelate to evaluate whether helical chirality could be induced in this manner. In this present experiment the complex **6a** was racemic. We are currently investigating other approaches to chiral induction.

(18) Hogg, R.; Wilkins, R. G. *J. Chem. Soc.* **1962**, 341.
(19) (a) Foley, J.; Tyagi, S.; Hathaway, J. *J. Chem. Soc., Dalton Trans.* **1984**, 1. (b) Hathaway, B. J.; Billing, D. E. *Coord. Chem. Rev.* **1970**, *5*, 143.

Scheme IV. Coordination Behavior of (Alkylthio)quinquepyridines and Inter-Relationships among Their Coordination Complexes

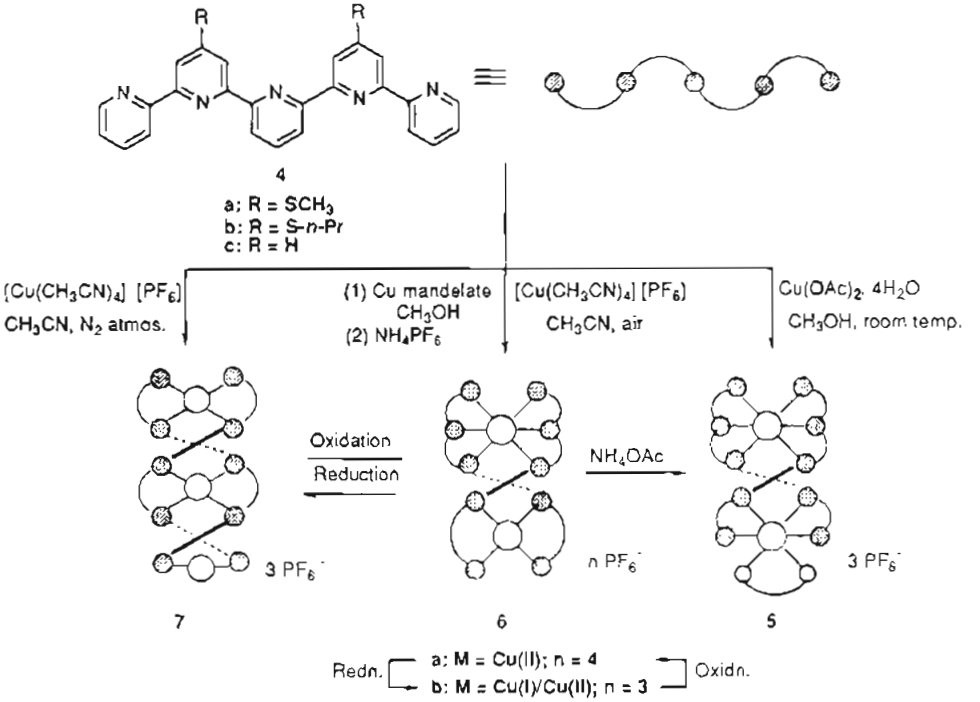

This unique 2-fold axis of symmetry is absent in the mixed-valence complex **6b**, whose X-ray-quality crystals crystallized as dark-red prisms from nitromethane by slow diffusion of diethyl ether. In this complex the distorted tetrahedron of Cu(1) has the following angles (deg): N(1)–Cu(1)–N(2), 80.2(2); N(2)–Cu(1)–N(2A), 124.8(2); N(2A)–Cu(1)–N(1A), 80.4(2); N(1A)–Cu(1)–N(1), 139.2(2). The distorted octahedron of Cu(2) has angles (deg) as follows: N(3a)–Cu(2)–N(4A), 75.3(2); N(4A)–Cu(2)–N(5A), 77.6(2); N(5A)–Cu(2)–N(5), 104.9(2); N(5)–Cu(2)–N(4), 78.1(2); N(4)–Cu(2)–N(3), 75.5(2); N(3A)–Cu(2)–N(3), 99.1(2).

Electrochemical Characterization. Mt-Quinquepyridine (4a): Cu Helicates. The cyclic voltammograms of the mixed-valence helicate $[Cu^{II}/Cu^{I}(mt\text{-}qnpy)_2][PF_6]_3$ (**6b**) and the homovalent Cu^{II}_2 helicate $[Cu^{II}(mt\text{-}qnpy)]_2[PF_6]_4$ (**6a**) in acetonitrile solution were found to be identical, as would be anticipated. In both cases, two one-electron, reversible waves were observed at –0.08 and +0.48 V, together with a small, additional wave at about +0.35 V. This additional wave is consistent with coordination by one or more acetonitrile molecules and was not observed in solvents of lesser coordinating ability such as DMF or DMSO. The cyclic voltammogram for $[Cu^{II}(mt\text{-}qnpy)]_2[PF_6]_4$ (**6a**) in 0.1 M TBAP/DMSO is shown in Figure 12.

The voltammetric responses of **6a,b** were also investigated with a rotating disk electrode (rde), this technique being chosen because, in the steady-state conditions imposed by the rde, the voltammetric response would yield important information regarding the oxidation states of the copper centers. The response at various rotation rates for a Pt rde in contact with a solution of **6a** in TBAP/MeCN was obtained. As the potential was scanned negatively from +0.80 V, two waves were observed at +0.48 and –0.08 V. In both cases, the current measured was cathodic, indicating that both waves were due to reduction processes, consistent with having both the copper centers present as Cu(II). In addition, Levich plots (i vs $\omega^{1/2}$) were linear, indicating mass transport control.

The current response at various rotation rates for a Pt rde in contact with a TBAP/MeCN solution of the mixed-valence complex **6b** was also obtained. In this case, while the current measured at –0.08 V was cathodic, indicative of a reduction process, the current measured at +0.45 V was anodic, indicating that an oxidation process was taking place in the latter case. Moreover, the measured current in the potential region between the two redox processes (+0.40 to +0.05 V) approached zero. These electrochemical data, when compared to the results obtained for the helicate **6a**, were indicative of a mixed-valence system and provided additional verification of the presence and stability of Cu(II)/Cu(I) in the complex **6b**.

The electrochemical response for the trimetallic helicate $\{Cu^{I}_3(mt\text{-}qnpy)_2][PF_6]_3$ (**7**) is presented in Figure 13. The helicate undergoes three sequential, one-electron, metal-based oxidations at –0.04, +0.50, and +1.03 V, providing convincing evidence for the presence of three metal centers. In addition, the fact that separate redox responses are observed for each of the metal centers suggests a significant degree of metal–metal interaction. In the negative potential region, all three helicates $[Cu^{II}(mt\text{-}qnpy)]_2[PF_6]_4$ (**6a**), $[Cu^{II}/Cu^{I}(mt\text{-}qnpy)]_2[PF_6]_3$ (**6b**), and $[Cu^{I}_3(mt\text{-}qnpy)_2][PF_6]_3$ (**7**) displayed almost identical voltammetric responses showing three reductions corresponding to ligand localized processes at –1.44, –1.62, and –1.88 V. All three complexes were generated both chemically and electrochemically, and electrochemical transformations were studied by spectroelectrochemistry as described below.

The electrochemical response of $[Cu^{II}_2(mt\text{-}qnpy)_2OAc][PF_6]_3$ (**5**) was dependent on the coordination ability of the solvent. In acetonitrile, the complex underwent two one-electron oxidations at –0.05 and +0.48 V corresponding to the Cu(I)/Cu(II) oxidation of the two metal centers. If the initial positive-going scan were reversed at +0.10 V, the first oxidation was reversible and the ratio of the peak current was equal to 1. If the scan were allowed to go beyond the second wave, e.g., to +0.06 V, upon scan reversal a small irreversible wave was observed at +0.10 V which could be due to a change in the coordination sphere around the Cu metal centers, probably involving one or more molecules of acetonitrile. With DMF as solvent the oxidations were slightly shifted to –0.02 and +0.49 V but, more importantly, they were both completely chemically reversible, again emphasizing the influence of the solvent in these processes. In the negative potential region there were two one-electron reductions at –1.53 and –1.72

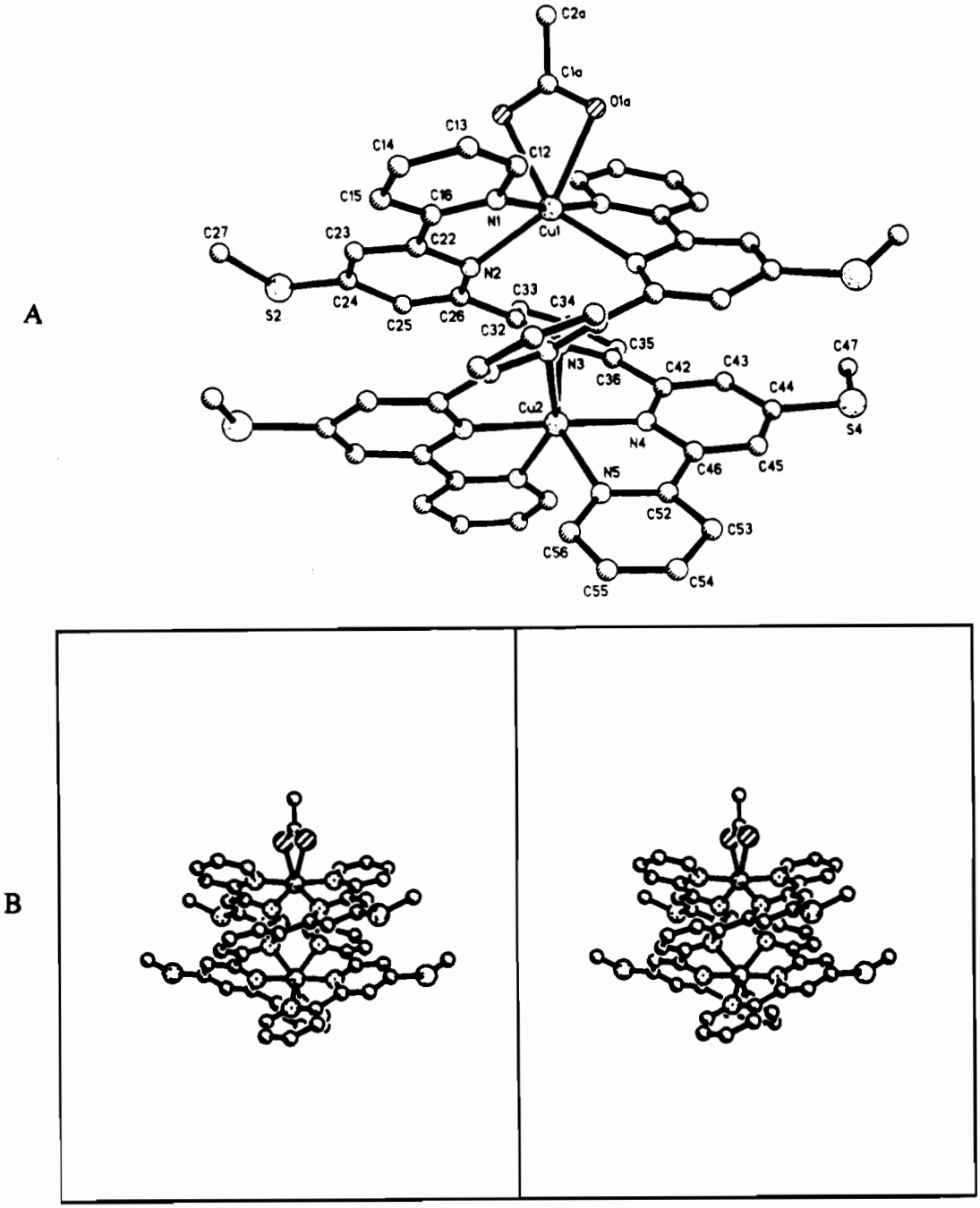

Figure 8. (A) X-ray structure of the right-handed (P) double-stranded helicate **5** derived from the ligand **4a**. (B) Stereotopic view of the helicate **5**.

V and a two-electron reduction at −1.99 V. These were all solvent dependent and are likely ligand-based reductions.

Comparison of the redox potentials of **5** with those of the acetate-free Cu(II) helicate **6a** (Table III) illustrates the effect of acetate, a σ-donor, shifting the oxidation potentials to less positive and the reductions to more negative potentials, as would be anticipated.

Spectroelectrochemical and Spectroscopic Measurements. Spectroelectrochemical techniques are particularly valuable in the study of these complexes since they allow monitoring of spectral changes as a function of applied potential. Figure 14 shows the visible spectrum of a solution of $[Cu^{II}(mt\text{-}qnpy)]_2[PF_6]_4$ (**6a**) taken every 3 min at an applied potential of +0.20 V. The dashed line (lower-most trace) represents the spectrum obtained prior to electrolysis. Upon application of a potential of +0.20 V to the working electrode, an absorption with a λ_{max} of 470 nm developed. The energy and shape of this absorption band were characteristic of the mixed-valence complex $[Cu^{II}/Cu^{I}(mt\text{-}qnpy)_2][PF_6]_3$ (**6b**), thus demonstrating that **6b** was generated upon electrolysis. When the applied potential was changed to −0.30 V, the absorption band at 470 nm shifted to 434 nm and a new band appeared at 550 nm. Both of these absorption bands are characteristic of the trimetallic complex $[Cu^{I}_3(mt\text{-}qnpy)_2][PF_6]_3$ (**7**). The visible spectrum measured after 1 h of electrolysis was found to be identical to that of an independently prepared sample of $[Cu^{I}_3(mt\text{-}qnpy)_2][PF_6]_3$ (**7**).

All of these processes were found to be reversible. For example, as the potential of the working electrode in contact with a solution of the trimetallic complex $[Cu^{I}_3(mt\text{-}qnpy)_2][PF_6]_3$ (**7**) was held at +0.20 V for 25 min there was a disappearance of the bands at 434 and 550 nm and the appearance of a new absorption at 470 nm. As mentioned before, the absorption band at 470 nm is characteristic of an MLCT transition of the mixed-valence complex $[Cu^{II}/Cu^{I}(mt\text{-}qnpy)_2][PF_6]_3$ (**6b**). As the applied potential was changed to +0.60 V, the absorption band at 470 nm decreased until it almost disappeared. The resulting spectrum was virtually identical to that of the dimeric complex $[Cu^{II}(mt\text{-}qnpy)]_2[PF_6]_4$ (**6a**). It is clear that both spectroelectrochemical

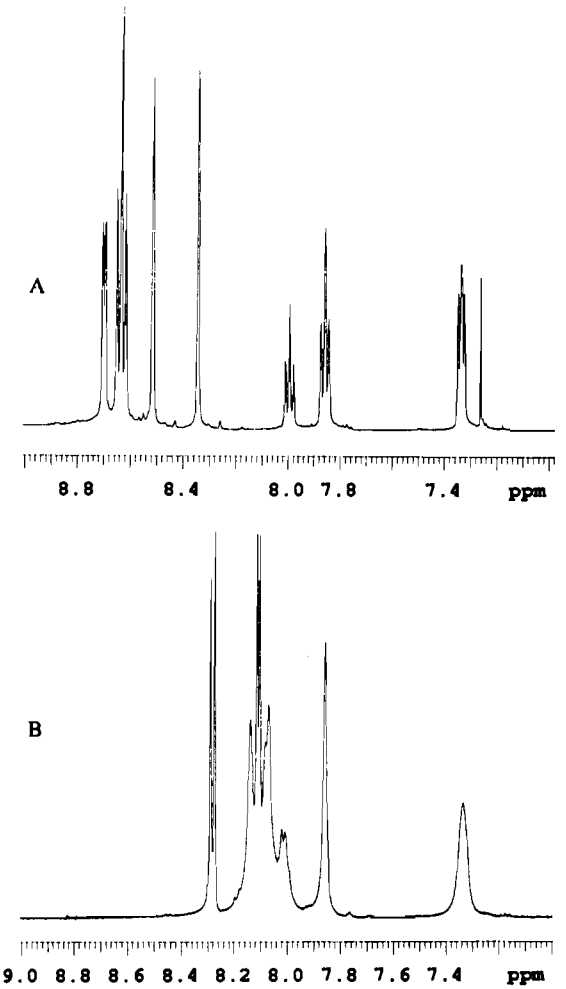

Figure 9. ^{1}H NMR spectrum (500 Mhz) of the aromatic region of (A) the ligand **4b** in $CDCl_3$ and (B) complex **7**, derived from **4b**, in acetone-d_6.

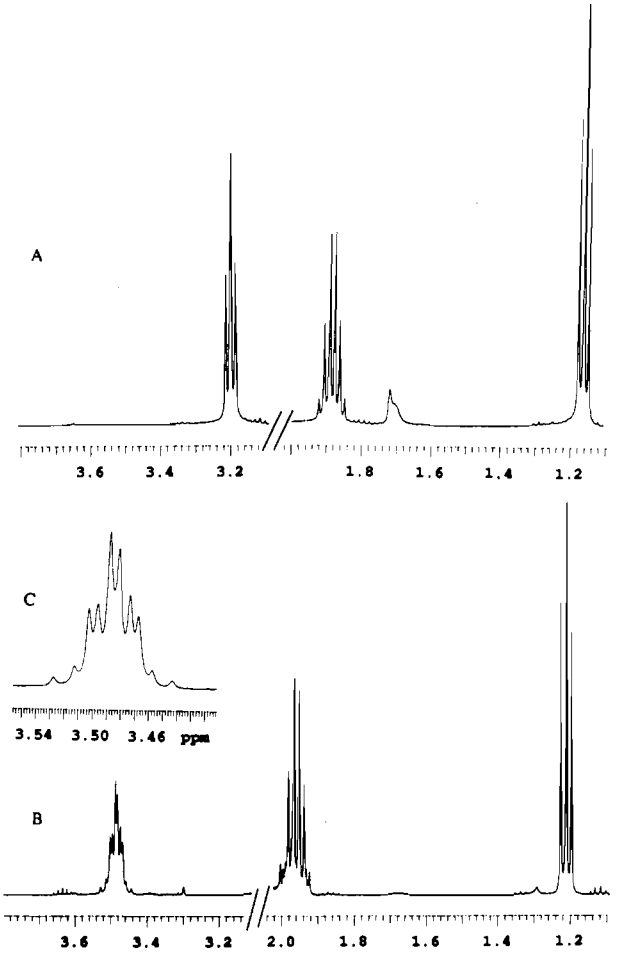

Figure 10. ^{1}H NMR spectra (500 MHz) of the aliphatic region of (A) the ligand **4b** in $CDCl_3$, (B) complex **7**, derived from **4b**, in acetone-d_6, and (C) expanded portion of SCH_2-group in the complex **7** at δ 3.48.

experiments yielded identical results, establishing the reversibility of these transformations.

In the near-IR region, an acetonitrile solution of the mixed-valence complex **6b** showed a broad absorption centered at 1414 nm [ϵ = 70 (cm M)$^{-1}$] which was absent in the spectrum of an acetonitrile solution of the homovalent bimetallic complex **6a**. This absorption, an intervalence electron-transfer transition between the mixed-valence copper centers, is clear evidence for electron delocalization and metal–metal coupling between the two copper centers in this complex.

Constable and co-workers[16] have previously reported on copper complexes of unsubstituted quinquepyridine **1c**. In those studies, they reported that the complex $[Cu_2L_2][PF_6]_3 \cdot 2CH_3CN$ (L = **1c**) exhibited two one-electron redox processes at +0.15 and –0.37 V vs ferrocene/ferrocenium (which correspond to about +0.60 and +0.08 V vs SSCE). Also, upon controlled-potential oxidation, the spectrum of the resulting product was similar to that of one of the isolated products which, on this basis, they ascribed to the Cu(II)/Cu(II) complex. They further reported that reduction of $[Cu_2L_2][PF_6]_3 \cdot 2CH_3CN$ (L = **1c**) resulted in the transfer of one electron but that no changes in the color of the solution were observed.

Because of the limited data and the fact that no voltammetric nor spectral scans are presented, it is somewhat difficult to compare directly our results with those mentioned above. However, our results on the mixed-valence and homovalence complexes **6b,a**, respectively, appear to be in reasonable agreement with those of Constable and co-workers.[15] However, the lack of spectral variations upon reduction of the mixed-valence complex is strongly at odds with our observations. Whereas we observe clean and reversible conversion to the trimetallic species $[Cu^I_3L_3]^{3+}$, they do not observe any spectral variations. In fact they appear to be unaware of the existence of this complex which we have prepared both by the electrochemical means mentioned above and chemically as described in the Experimental Section. We cannot reconcile our observations with theirs, but it is possible that the materials that they employed could be contaminated since as they state "... the products could be separated by hand from the mixture of crystals". It is also possible (although it is difficult to ascertain) that their use of the unsubstituted ligand **1c** gives rise to complexes with significantly different reactivity.

The complexes that we have prepared and characterized, however, exhibit very rich redox chemistry including the aforementioned reversible, redox-induced structural changes.

Conclusions

A variety of double-stranded copper helicates have been synthesized from alkylthio-substituted quaterpyridine and quinquepyridines. The thioalkyl groups favor the solubility requirement that facilitates self-assembly processes under gentle conditions, resulting in only one type of complex in quantitative yield, and provide a convenient ^{1}H NMR means of establishing solution stability and the chiral nature of the complexes. There is no evidence from our study that the sulfur atoms compete as ligating centers or adversely affect the coordination behavior of the these ligands. No electrochemical oxidations of these sulfurs were observed over the potential range used to study the redox properties of the metal centers. Two principal coordination geometries (tetrahedral and octahedral) were involved in these helicates as well as combinations of tetrahedral/octahedral and tetrahedral/linear geometries. In addition, a unique trimetallic mt-quin-

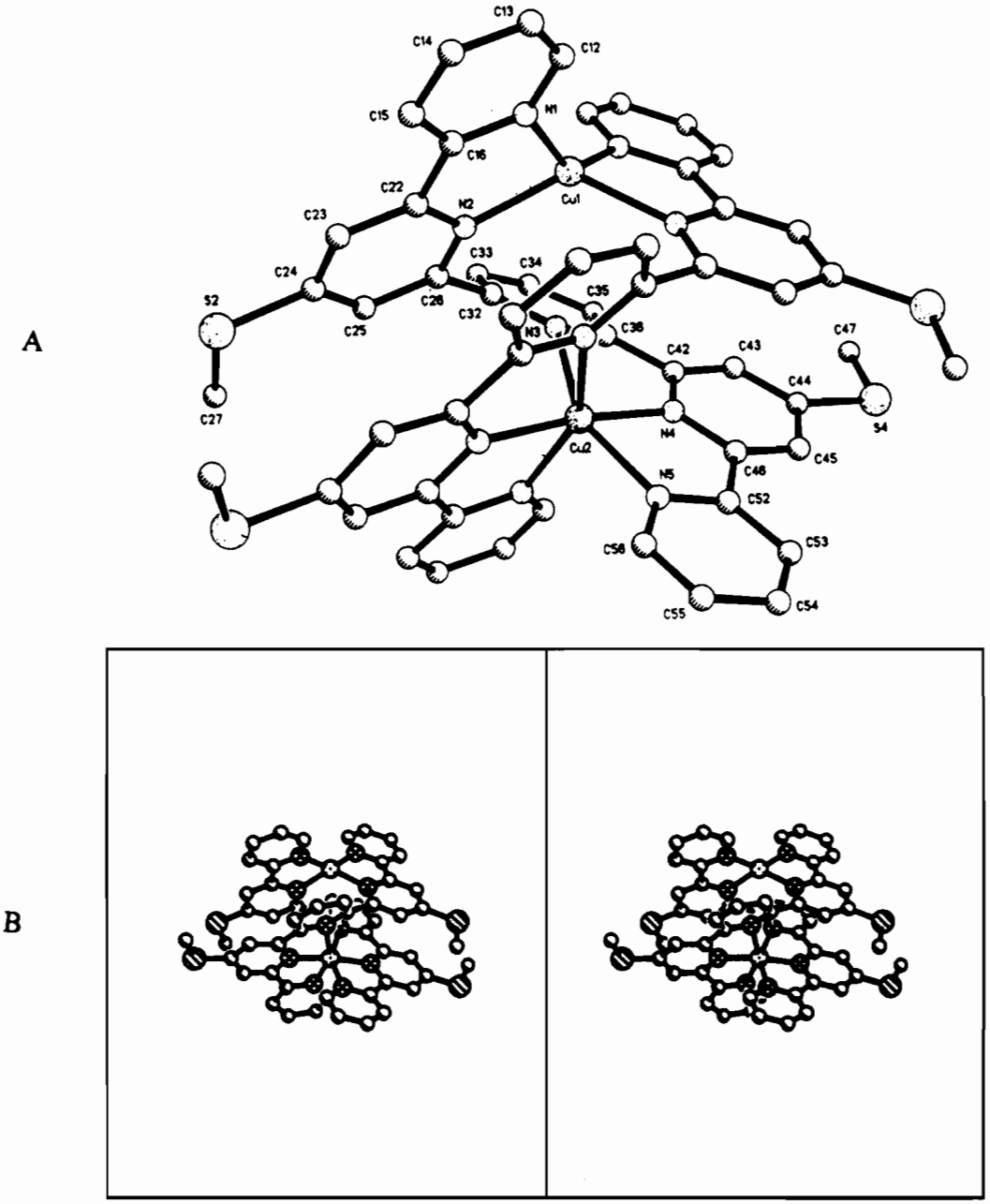

Figure 11. (A) X-ray structure of the right-handed (P) mixed-valence double-stranded helicate **6b** derived from the ligand **4a**. (B) Stereotopic view of the helicate **6b**.

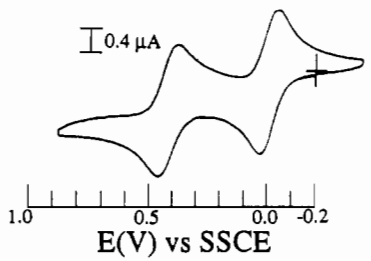

Figure 12. Cyclic voltammogram for $[Cu^{II}(mt\text{-}qnpy)]_2[PF_6]_4$ (**6a**) in 0.1 M TBAP/DMSO.

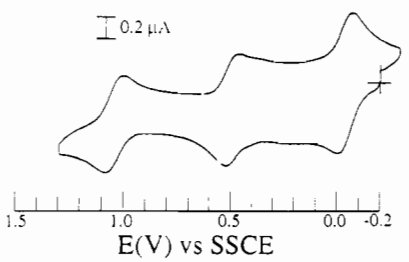

Figure 13. Cyclic voltammogram for $[Cu^{I}_3(mt\text{-}qnpy)_2][PF_6]_3$ (**7**) in 0.1 M TBAP/CH_3CN.

quepyridine complex has been prepared that shows significant metal–metal interaction, clearly evident from the three, sequential one-electron, metal-based oxidations. In many cases, dramatic (and often reversible) changes in the coordination geometry could be elicited upon changes in oxidation state. The rate of these changes and the stability of the intermediates were strongly dependent on the ligand. For example, reduction of the monomeric species $[Cu^{II}(mt\text{-}qtpy)]^{2+}$ resulted in rapid generation of the dimer $[Cu^{I}(mt\text{-}qtpy)]_2^{2+}$. This dimer could be oxidized in a two-electron step to yield the initial monomeric species. These transformations were very rapid so that only when using very fast rates of potential sweep (4 kV/s) could intermediate species be detected. However, the reversibility of these changes could be further corroborated by spectroelectrochemical measurements. The closely related species $[Cu^{II}(CH_3)_4\text{-}qtpy]$ (**3a**) undergoes the monomer/dimer transformation, but once formed, the dimer is stable and exhibits two one-electron oxidations. Because this is a symmetric species, this can be used as evidence of metal–metal interaction. It is

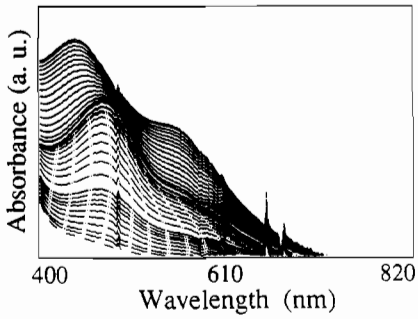

Figure 14. Visible spectra at 3-min intervals of $[Cu^{II}(mt\text{-}qnpy)]_2[PF_6]_4$ (**6a**) prior to (lower-most trace, - - -) and after (—) electrolysis at an applied potential of +0.20 V for 30 min and −0.30 V for 30 min in 0.1 M TBAP/CH_3CN.

quite likely that the dimeric species $[Cu^{I}(mt\text{-}qtpy)]_2^{2+}$ exhibits metal–metal interaction; however, the rapid dimer/monomer interconversions preclude the use of electrochemical techniques to ascertain this effect.

The mt-qnpy complexes also undergo redox state dependent changes in their geometry. In this case the processes involve dimetallic/trimetallic transformations with some of the intermediate species being stable. For example both the Cu(II)/Cu(II) and the mixed-valence dimer Cu(II)/Cu(I) are stable. However, the Cu(I)/Cu(I) species rapidly converts into a trimetallic system. Such behavior might be indicative of the fact that in a dimeric species the mt-qnpy ligand can accommodate both 6- and 4-coordinate species so that the mixed-valence dimer is stable. However, generation of the Cu(I)/Cu(I) species rapidly yields the trimetallic species. Further stabilization of this trimetallic species in solution by the introduction of phenyl substituents into the 2-positions of the terminal pyridine rings, as in the terpy system described earlier,[11] is currently being investigated.

The mixed-valence Cu(II)/Cu(I) complex **6b** exhibits a transition in the near-infrared that we ascribe to an intervalence transfer (IT) transition and which we take as an indication of metal–metal interactions. Even though the complex also exhibits two one-electron oxidations, the fact that the coordination environment around each metal center is different precludes the use of electrochemical techniques as evidence of metal–metal interactions. However, the presence of the IT band represents compelling evidence of such interactions.

Because of the variety of structures that can be generated and the changes elicited by variations in their redox state, these compounds could, in principle, be used for recognition purposes on the basis of oxidation state and as triggers in chemical reactions as well as in other technological applications. We are currently studying these possibilities as well as extending our work to include tetrametallic and pentametallic representatives of this series.

Acknowledgment. We thank Dr. R. Kullnig for his interest and encouragement during the X-ray structural determinations and the NSF (Grant CHE-9105906) and USPHS (Grant S10RR06245) for funds for the purchase of the 500-MHz NMR spectrometer. FAB mass spectral data were obtained by Dr. R. Milberg, University of Illinois. Partial support of this work by the American Cyanamid Company (K.T.P.) and by the Materials Science Center at Cornell University (C.R.A. and H.D.A.) is gratefully acknowledged. We also thank K. Trible for her help in the fast scan cyclic voltammetric measurements.

Supplementary Material Available: Tables providing full details of the X-ray structural determinations including crystal Data, atomic coordinates and isotropic thermal parameters, bond lengths, bond angles, anisotropic thermal parameters, H-atom coordinates, and isotropic thermal parameters for complexes **2b**, **5b**, and **6** (24 pages). Ordering information is given on any current masthead page.